# Title

Cross-species functional diversity within the PIN auxin efflux protein family

# Authors

Devin Lee O'Connor[1,^], Samuel Elton[1*], Fabrizio Ticchiarelli[1*], Mon Mandy Hsia[2], John Vogel[3,4], Ottoline Leyser[1].

# Affiliations

[1]Sainsbury Laboratory University of Cambridge, Cambridge, UK.

[2]USDA-ARS Western Regional Research Center, Albany, CA.

[3]U.S. Department of Energy Joint Genome Institute, Walnut Creek, CA.

[4]Department of Plant and Microbial Biology, University of California, Berkeley, CA.

*These authors contributed equally.

^Author for Correspondence: Devin Lee O'Connor devin.oconnor@slcu.cam.ac.uk

## Abstract

In Arabidopsis, development during flowering is coordinated by transport of the hormone auxin mediated by polar-localized PIN-FORMED1 (AtPIN1). However, Arabidopsis has lost a PIN clade sister to AtPIN1, Sister-of-PIN1 (SoPIN1), which is conserved in flowering plants. We previously proposed that the AtPIN1 organ initiation and vein patterning functions are split between the SoPIN1 and PIN1 clades in grasses. Here we show that in the grass Brachypodium *sopin1* mutants have organ initiation defects similar to Arabidopsis *atpin1*, while loss of *PIN1* function in Brachypodium has little effect on organ initiation but alters stem growth. Heterologous expression of Brachypodium SoPIN1 and PIN1b in Arabidopsis provides further evidence of functional specificity. SoPIN1 but not PIN1b can mediate flower formation in null *atpin1* mutants, although both can complement a missense allele. The behavior of SoPIN1 and PIN1b in Arabidopsis illustrates how membrane and tissue-level accumulation, transport activity, and interaction contribute to PIN functional specificity.


## Introduction

The plant hormone auxin is an essential mobile signal controlling growth and patterning throughout plant development (Leyser, 2010). Auxin can passively enter cells, triggering a vast array of downstream signaling events (Wang and Estelle, 2014), but it cannot easily exit the cell without active transport (Raven, 1975; Rubery and Sheldrake, 1974). As a result, directional efflux mediated by the polar-localized PIN-FORMED (PIN) efflux carriers can organize auxin flows and accumulation patterns, creating concentration maxima and paths of transport that regulate growth, position organs, and pattern tissues

39 (Adamowski and Friml, 2015). Because auxin itself feeds back to regulate PIN-mediated
40 transport both transcriptionally and post-transcriptionally (Leyser, 2006), the transport
41 system shows remarkable robustness and plasticity. For example, compensatory
42 changes in PIN abundance between PIN family members can mitigate PIN loss-of-
43 function mutant phenotypes (Blilou et al., 2005; Paponov et al., 2005; Vieten et al.,
44 2005), environmental inputs can trigger tissue-level changes in PIN abundance and
45 polarity leading to altered plant growth (Habets and Offringa, 2014), and auxin transport
46 paths can be reorganized in response to injury (Sauer et al., 2006; Xu et al., 2006), or
47 spontaneously in tissue culture (Gordon et al., 2007). The self-organizing properties of
48 the auxin transport system thus gives this patterning mechanism extraordinary
49 versatility, and allows it to coordinate both local and long-range communication in
50 plants.

51 The correct initiation and positioning of organs (leaves, flowers, stems) in the growing
52 tip, or shoot apical meristem, of *Arabidopsis thaliana* (Arabidopsis) plants requires the
53 action of the PIN-FORMED1 (AtPIN1) auxin efflux carrier (Okada et al., 1991). AtPIN1
54 is targeted to the plasma membrane and polarized in cells (Gälweiler et al., 1998). In
55 the meristem epidermis, polarization of AtPIN1 in neighboring cells converges around
56 the initiation sites of new organs, suggesting that polarized AtPIN1 concentrates auxin
57 into local maxima causing organ initiation (Benková et al., 2003; Heisler et al., 2005;
58 Reinhardt et al., 2003). Accordingly, in *atpin1* loss-of-function mutants, or if auxin
59 transport is pharmacologically inhibited, organ initiation is aborted, but it can be rescued
60 with local auxin application to the meristem flank (Reinhardt et al., 2003; Reinhardt et
61 al., 2000). Organ initiation in *atpin1* mutants can also be rescued with epidermal-specific

62 AtPIN1 expression (Bilsborough et al., 2011), and reducing AtPIN1 function specifically
63 in the epidermis compromises organ positioning and initiation (Kierzkowski et al., 2013),
64 demonstrating the importance of convergent AtPIN1 polarization in the epidermis during
65 organ formation.

66 The recurrent formation of AtPIN1 convergence points surrounding auxin maxima in the
67 meristem epidermis has been the focus of several computational models that attempt to
68 explain how auxin feeds back on its own transport via AtPIN1 to concentrate auxin and
69 control organ spacing (Abley et al., 2016; Bayer et al., 2009; Bhatia et al., 2016; Heisler
70 et al., 2010; Jönsson et al., 2006; Smith et al., 2006; Stoma et al., 2008). However,
71 AtPIN1 is also expressed during the patterning of the vascular strands formed
72 coincident with organ positioning, and in these sub-epidermal cells AtPIN1 is polarized
73 rootward, away from the presumed auxin maxima, suggesting that AtPIN1 polarity with
74 respect to auxin concentration may vary across tissues or over developmental time
75 (Bayer et al., 2009).

76 Indeed, AtPIN1 has several functions post organ initiation that are not necessarily
77 associated with convergent polarization patterns (Gälweiler et al., 1998; Scarpella et al.,
78 2006). AtPIN1 is not required for organ formation during the vegetative phase. Mutants
79 lacking AtPIN1 form leaves, but they are misplaced and have severe morphological and
80 vascular defects similar to those observed upon pharmacological inhibition of auxin
81 transport, suggesting an important role for AtPIN1 in post-initiation morphogenesis and
82 vein patterning in leaves (Guenot et al., 2012; Sawchuk et al., 2013; Verna et al., 2015).
83 Furthermore, in mature tissues, AtPIN1 is polarized rootward in vascular-associated
84 cells and is required for efficient long distance transport of auxin down the shoot in the

85 polar auxin transport stream, and this has been proposed to play an important role in
86 the regulation of shoot branching (Bennett et al., 2016; Bennett et al., 2006; Gälweiler et
87 al., 1998; Shinohara et al., 2013). Mutations in other PIN family members in
88 combination with *atpin1* mutants suggest further functions in embryo development, root
89 development and during plant growth responses to light and gravity (Leyser, 2005).
90 Unfortunately, the myriad roles for AtPIN1 during inflorescence development are
91 genetically obscured by the severity of *atpin1* organ initiation defects.

92 We previously showed that all sampled flowering plants outside of the Brassicacea
93 family have a clade of PIN proteins phylogenetically sister to the PIN1 clade (The Sister-
94 of-PIN1 or SoPIN1 clade), while Arabidopsis and other Brassicacea species have lost
95 this clade (O'Connor et al., 2014). During organ initiation in the grass *Brachypodium*
96 *distachyon* (Brachypodium) which has both PIN1 and SoPIN1 clades, SoPIN1 is highly
97 expressed in the epidermis, polarizes towards presumed auxin maxima, and forms
98 convergent polarization patterns during the formation of new organs, suggesting a role
99 in creating the auxin maxima required for organ initiation. In contrast, the duplicate
100 Brachypodium PIN1 clade members, PIN1a and PIN1b, are not highly expressed in the
101 epidermis, orient away from presumed auxin maxima, and are primarily expressed
102 during patterning in the sub-epidermal tissues. Thus, the combined expression domains
103 and polarization behaviors of SoPIN1, PIN1a, and PIN1b in Brachypodium largely
104 recapitulate those observed for AtPIN1 alone in Arabidopsis.

105 The dynamic localization and polarization patterns of the Brachypodium SoPIN1 and
106 PIN1 clades can be modeled with two different polarization modes with respect to auxin.
107 PIN behaviors can be captured by a model in which SoPIN1 polarizes “up-the-gradient”,

108 towards the neighboring cell with the highest auxin concentration, while PIN1a and
109 PIN1b polarize “with-the-flux”, accumulating in the membrane with the highest net auxin
110 efflux (O'Connor et al., 2014). Both polarization modes were previously applied to
111 AtPIN1 in order to capture the switch in polarity observed during organ initiation and
112 vein patterning, first orienting toward the auxin maximum during convergence point
113 formation, then orienting away from the maximum below the epidermis during vein
114 patterning (Bayer et al., 2009). These localization and modeling results suggest that in
115 most angiosperm species the organ placement and vascular patterning functions
116 attributed to AtPIN1 in Arabidopsis are split between the PIN1 and SoPIN1 clades, and
117 that these two clades have different polarization properties with respect to auxin.

118 Exploring this hypothesis, here we present the functional analysis of both the SoPIN1
119 and PIN1 protein clades in Brachypodium, a species with the canonical two-clade family
120 structure. We show that SoPIN1 and the PIN1 clade members PIN1a and PIN1b have
121 different functions during Brachypodium development, with SoPIN1 being required for
122 organ initiation during the flowering phase, and PIN1a and PIN1b regulating stem
123 growth. Using heterologous expression in Arabidopsis, we show that the SoPIN1 and
124 PIN1b proteins have different accumulation, polarization, and transport behaviors that
125 result in different functional properties independent of transcriptional context. In addition
126 to elucidating several ways in which PIN family members can be functionally distinct,
127 these results suggest that the Arabidopsis AtPIN1 protein represents an example of an
128 evolutionary phenomenon the opposite of subfunctionalisation in which protein functions
129 are amalgamated into a single protein rather than diversified amongst paralogs. AtPIN1

130 has a repertoire of roles, and associated polarization behaviors that are distributed
131 among several clades of PIN proteins in most flowering plants.

132

# 133 Results

## 134 The SoPIN1 and PIN1 clades have different functions in 135 Brachypodium

136 We targeted Brachypodium SoPIN1, PIN1a, and PIN1b with gene-specific Clustered
137 Regularly Interspaced Short Palindromic Repeats (CRISPR) and for all three genes
138 recovered independent single base-pair lesions causing frame shifts and premature
139 stop codons (Figure 1A). The wild-type Brachypodium inflorescence meristem normally
140 makes several lateral spikelet meristems (lsm), before producing a terminal spikelet
141 meristem (tsm) (Figure 1B)(Derbyshire and Byrne, 2013). Both lateral and terminal
142 spikelet meristems are consumed in the production of florets (Figure 1D, 1F). The
143 *sopin1-1* inflorescence meristems had severe organ and spikelet branch initiation
144 defects (Figure 1C), which resulted in reduced total whole-plant spikelet number (Figure
145 1H). When spikelets did form, *sopin1-1* spikelet meristems were often devoid of new
146 organs (Figure 1E), and very few recognizable florets were produced (Figure 1I). In
147 support of the *sopin1-1* lesion being responsible for these varied inflorescence
148 phenotypes, we complemented inflorescence development and seed set by crossing
149 *sopin1-1* to the previously published SoPIN1-CITRINE fusion line (Figure 1 –
150 supplement 1)(O'Connor et al., 2014). The pleotropic defects displayed by *sopin1-1* in

151 the inflorescence are remarkably similar to loss-of-function *pin1* mutants in *Arabidopsis*
152 (Okada et al., 1991) and *Cardamine hirsuta* (Barkoulas et al., 2008).

153 In wild-type spikelet meristems, SoPIN1 convergence point formation is coincident with
154 an increase in the auxin signaling reporter DR5 (O'Connor et al., 2014), as well as a
155 decrease in the nuclear auxin response reporter protein DII-Venus (Brunoud et al.,
156 2012) (DII) (Figure 1J), which functions in Brachypodium and is degraded in the
157 presence of auxin in spikelet meristems (Figure 1 - supplement 2). In *sopin1-1*
158 meristems, DII accumulation was uniformly high for long stretches of the epidermis, and
159 the patterned reduction of DII both in the meristem epidermis and internally failed to
160 occur, suggesting a failure to organize auxin maxima (Figure 1K arrow).

161 In contrast to the severe defects of *sopin1-1*, organ initiation in *pin1a-1* and *pin1b-1*
162 single mutants was largely unaffected. The mature inflorescences of both *pin1a-1* and
163 *pin1b-1* had normal spikelets (Figure 1F), and spikelet meristem morphology was
164 indistinguishable from wild-type (Figure 1G). Mutant *pin1a-1* plants appeared visually
165 wild-type, but we measured a slight increase in total spikelet number (Figure 1H).
166 Mutant *pin1b-1* plants were similar to wild-type with respect to both spikelet and floret
167 numbers (Figure 1H, 1I), but often had bent apical internodes (Figure 1F arrowhead).
168 While *pin1a-1* and *pin1b-1* single mutants had no clear organ initiation defects they
169 showed changes in internode length (Figure 2). Plant stature in *pin1a-1* mutants was
170 largely indistinguishable from wild-type (Figure 2B), but we measured a small reduction
171 in the length of the I4 internode (Figure 2E). In contrast, *pin1b-1* plants were easily
172 distinguished from wild-type because of a significant increase in internode length at the
173 base of the plant, resulting in greater overall plant height (Figure 2E). The elongated

174 basal internodes and bent stems of *pin1b-1* resulted in a less compact plant architecture
175 compared to the other genotypes (Figure 2C). The increase in basal internode length in
176 *pin1b-1* single mutants was rescued by the previously published PIN1b-CITRINE
177 florescent reporter (O'Connor et al., 2014) (Figure 2 – supplement 1).

178 The PIN1a and PIN1b duplication is specific to, but conserved within the grasses
179 (O'Connor et al., 2014). Thus, we suspected these two genes would show a degree of
180 genetic redundancy. Indeed, *pin1a-1/pin1b-1* (*pin1a/b*) double mutants showed a
181 synergistic phenotype, with severely reduced plant height (Figure 2D), resulting
182 primarily from reduced internode growth in the upper internodes (Figure 2E). However,
183 despite loss of both PIN1a and PIN1b function, *pin1a/b* double mutants made normal
184 spikelet meristems (Figure 1G), had a wild-type total spikelet number (Figure 1H), and
185 showed only a small reduction in floret number in the terminal spikelet (Figure 1I). In
186 addition, unlike *sopin1-1* plants, *pin1a/b* double mutants set ample seed.

187 Combined these phenotypes provide further support for functional distinction between
188 the SoPIN1 and PIN1 clades, and indicate that while the PIN1 clade is expendable for
189 organ initiation in Brachypodium, it is involved in the regulation of internode growth.

190

## 191 AtPIN1, SoPIN1, and PIN1b accumulate differently in Arabidopsis
## 192 under the same transcriptional control

193 During organ formation in the Brachypodium shoot, expression of both SoPIN1 and
194 PIN1b precedes PIN1a, which only accumulates significantly at the sites of vein

195 formation after the organs begin to grow (O'Connor et al., 2014). In the earliest stages
196 of initiation, prior to the periclinal cell divisions that are the hallmark of morphogenesis,
197 SoPIN1 forms convergent polarization patterns around the presumed auxin maxima in
198 the meristem epidermis, while PIN1b is expressed internally and orients away from the
199 maxima (O'Connor et al., 2014). Because of their early expression, opposing
200 polarization patterns, and their clear single-mutant phenotypes in Brachypodium, we
201 focused on characterizing SoPIN1 and PIN1b as representatives of the SoPIN1 and
202 PIN1 clades.

203 The difference between the *sopin1-1* and *pin1b-1* phenotypes in Brachypodium could
204 be due to their different expression patterns and not necessarily to differences in their
205 polarization with respect to auxin concentration or flux as previously hypothesized
206 (O'Connor et al., 2014). In order to assess the functional differences between the
207 proteins, independent of transcriptional context, we expressed both Brachypodium
208 proteins tagged with CITRINE (a YFP derivative) in wild-type Arabidopsis (Columbia,
209 Col-0) under the control of a 3.5kb Arabidopsis *PIN1* promoter fragment which includes
210 sequences known to drive PIN1 expression sufficient to complement *pin1* mutants
211 (*proAtPIN1*) (Benková et al., 2003; Heisler et al., 2005). In the Arabidopsis inflorescence
212 meristem, wild-type AtPIN1 forms convergent polarization patterns that mark the sites of
213 initiating flower primordia (Figure 3A). Remarkably, despite the loss of the SoPIN1 clade
214 from Arabidopsis, Brachypodium SoPIN1 also created clear convergent polarization
215 patterns in Arabidopsis inflorescence meristems but was less abundant in the central
216 domain of the apical dome (Figure 3B, 25 of 27 meristems from 4 independent
217 transgenic events). Similar to AtPIN1, SoPIN1 protein abundance was highest in the

218 meristem epidermis, and SoPIN1 convergence points were most clearly observed
219 surrounding I2 and I1 primordia (Figure 3B). Below the epidermis wild-type AtPIN1
220 accumulates in small groups of cells that will become the vasculature (Figure 3 –
221 supplement 1 panel A arrows). In contrast, sub-epidermal SoPIN1 accumulated in an ill-
222 defined ring shape surrounding the meristem central domain without distinct foci of
223 expression (Figure 3 – supplement 1 panel B, 15 of 23 meristems from 4 independent
224 transgenic events).

225 In contrast to both AtPIN1 and SoPIN1, under the same promoter significant PIN1b
226 accumulation was absent from the meristem epidermis in 19 of 29 meristems from 7
227 independent transgenic events. In the few meristems where PIN1b accumulated in the
228 epidermis, it did not show clear convergent polarization patterns, and its polarity was
229 often unclear (Figure 3C). Within initiating organs, PIN1b often localized to punctate
230 vesicular bodies inside cells, not in the cell membrane (Figure 3C arrowhead). PIN1b
231 accumulation remained low just below the meristem apex, but in contrast to SoPIN1,
232 PIN1b formed defined domains around the presumptive developing vascular bundles
233 similar to AtPIN1 (Figure 3 – supplement 1 panel C arrows). The lack of PIN1b protein
234 in the meristem epidermis was not due to silencing of the transgene in these lines
235 because we observed abundant PIN1b protein in the developing vasculature below the
236 apex, even in plants where the meristem had no detectable epidermal expression
237 (Figure 3F) (8 samples from 4 events). In contrast, AtPIN1 and SoPIN1 accumulated in
238 both the vasculature and the epidermis in these more mature tissues (Figure 3D, 3E),
239 although SoPIN1 seemed more abundant in the epidermis than AtPIN1 (see arrows)
240 (SoPIN1 - 5 samples from 2 events).

241 In order to determine whether there were similar tissue-level differences in protein
242 accumulation in mature tissues, where AtPIN1 is implicated in branch control, we
243 imaged AtPIN1, SoPIN1, and PIN1b in the basal internode in mature plants 1cm above
244 the rosette. Here, AtPIN1 normally accumulates in a highly polar manner in the rootward
245 plasma membranes of cambium (ca) and xylem parenchyma (xp) vascular-associated
246 tissues (Figure 3G, 3J) (Bennett et al., 2016; Gälweiler et al., 1998). Here PIN1b
247 accumulated in a similar pattern to AtPIN1 (Figure 3I, 3L. 10 samples from 5 events). In
248 contrast, in addition to accumulating in the cambium and xylem parenchyma, SoPIN1
249 accumulated in the mature cortex (co) and central pith tissues (p) (Figure 3H, 3K. 15
250 samples from 4 events). AtPIN1 is not normally observed in the mature cortex or pith
251 tissues (Figure 3G, 3J) (Bennett et al., 2016; Gälweiler et al., 1998). However, we
252 detected abundant AtPIN1 expression in the immature pith closer to the apex (Figure
253 3D box, Figure 3 – supplement 1 panel D), suggesting that *proAtPIN1* initially drives
254 expression in a broad domain and that AtPIN1 and PIN1b are both cleared from the
255 cortex and pith by maturity, while SoPIN1 is not. In the basal internode all three proteins
256 showed the characteristic rootward polarization pattern regardless of tissue-level
257 abundance (Figure 3 – supplement 1 panels D, E, F arrows).

258 Taken together, these results show that even under the same transcriptional control
259 AtPIN1, SoPIN1, and PIN1b show distinct tissue-level accumulation patterns in
260 Arabidopsis. While the overall behavior of the two Brachypodium proteins is similar to
261 AtPIN1 in many tissues, there are behaviors unique to each. PIN1b fails to accumulate
262 in epidermal tissues where AtPIN1 and SoPIN1 remain high, whereas SoPIN1
263 accumulates in the mature cortex and pith tissue where AtPIN1 and PIN1b do not. The

264 convergent polarization patterns of SoPIN1 and the vascular accumulation of PIN1b in
265 Arabidopsis are remarkably similar to their native behaviors in Brachypodium (O'Connor
266 et al., 2014), suggesting protein-intrinsic features might control tissue level
267 accumulation in the two species.

268

## 269 SoPIN1 but not PIN1b can restore organ initiation and bulk auxin 270 transport in AtPIN1 null mutants

271 To determine whether the observed differences in SoPIN1 and PIN1b polarization and
272 accumulation have functional consequences in Arabidopsis, we used the *proAtPIN1*-
273 driven SoPIN1 and PIN1b constructs to complement the Arabidopsis *pin1-613* mutant
274 (also known as *pin1-7)*. The *pin1-613* allele is a putative null T-DNA insertion allele with
275 severe organ initiation defects in the inflorescence (Absmanner et al., 2014; Bennett et
276 al., 2006; Smith et al., 2006). Given that epidermal AtPIN1 function is important for
277 organ initiation (Bilsborough et al., 2011; Kierzkowski et al., 2013), as expected only
278 SoPIN1 and not PIN1b was able to complement the *pin1-613* mutation and mediate
279 organ initiation (Figure 4A) (3 out of 6 independent transgenic events showed
280 complementation). However, phenotypic complementation of *pin1-613* by SoPIN1 was
281 incomplete, and mature plants showed a variety of phenotypic defects (Figure 4A,
282 Figure 4 - supplement 1). Most notably, each flower produced more sepals and petals
283 than wild-type but almost no stamens (Figure 4C, Figure 4 - supplement 2). SoPIN1-
284 complemented *pin1-613* plants were thus sterile. We wondered whether these
285 phenotypes could be explained by poor auxin transport function of SoPIN1 in

286 Arabidopsis. However, SoPIN1 restored wild-type levels of bulk auxin transport to *pin1-*
287 *613* basal internodes (Figure 4D). Thus, SoPIN1 is capable of supporting organ
288 initiation and mediating rootward auxin transport in the stem, but it is not functionally
289 identical to AtPIN1 expressed under the same promoter.

290 In SoPIN1-complemented *pin1-613* mutants, SoPIN1 protein accumulation in the
291 meristem epidermis was higher than that observed in a wild-type or heterozygous
292 genetic background, and the pronounced convergent polarization patterns observed in
293 the wild-type background were less defined (Figure 5A, Figure 5 - supplement 1) (16 of
294 16 meristems). SoPIN1-complemented meristems showed a variety of phyllotactic
295 defects and had highly variable morphologies (Figure 5 – supplement 1 panel B) (16 of
296 16 meristems). Similar to the pattern observed in the wild-type background, sub-
297 epidermal SoPIN1 in *pin1-613* mutants accumulated in a loosely defined ring within
298 which individual vein traces were difficult to discern (Figure 5I) (13 of 16 meristems). In
299 mature tissues, SoPIN1 accumulated in the epidermis, vasculature, and pith similar to
300 the wild-type background (Figure 5C, 5E, 5G).

301 In contrast to SoPIN1, PIN1b-expressing *pin1-613* plants had pin-formed inflorescences
302 that were indistinguishable from *pin1-613* alone (Figure 4A) (all 10 expressing events
303 failed to complement). The lack of complementation mediated by PIN1b was not caused
304 by silencing or low expression level because abundant PIN1b signal was observed in
305 *pin1-613* meristems (23 of 26 *pin1-613* meristems from 7 events). In contrast to the
306 wild-type background, most PIN1b expressing *pin1-613* samples had abundant
307 epidermal expression, forming a ring-shaped domain around the meristem apex (Figure
308 5B, 5D arrow, Figure 5 - supplement 2) (14 of 19 meristems from 6 events). Also unlike

309 the wild-type background, PIN1b in the epidermis of *pin1-613* meristems was more
310 consistently targeted to the membrane, and was often polar (Figure 5K). However, even
311 with this elevated polar expression in the meristem epidermis, PIN1b was unable to
312 mediate organ initiation in *pin1-613* mutants. Below the apex, PIN1b was polarized
313 rootward in *pin1-613* meristems (Figure 5J), forming defined traces associated with the
314 vasculature (Figure 5F, 5L). In the basal stem of *pin1-613* mutants PIN1b accumulated
315 in a pattern similar to wild-type, although the arrangement of vascular bundles was
316 irregular (Figure 5H). Remarkably, despite clear polar PIN1b expression in *pin1-613*
317 mutant stems (Figure 5M), PIN1b was unable to rescue bulk auxin transport in this
318 tissue (Figure 4D).

319 Although PIN1b was incapable of supporting organ formation or mediating bulk
320 transport in *pin1-613,* when an auxin maximum was created artificially by addition of
321 lanolin paste infused with IAA, PIN1b epidermal accumulation increased during the
322 initiation of the resultant primordia (Figure 5 – supplement 3) (4 of 6 samples from 2
323 independent transgenic events). Thus, in the absence of AtPIN1, PIN1b accumulation in
324 the epidermis is still auxin responsive and capable polar localization, but it is not able to
325 mediate organ initiation itself. Consistent with this result, it appears to be unable to
326 transport auxin.

327 Because PIN1b seemed to form more defined sub-epidermal traces than SoPIN1
328 (Compare Figure 3 – supplement 1 panels B and C, and Figure 5I and 5L) we thought
329 PIN1b combined with SoPIN1 may improve the partial SoPIN1-mediated
330 complementation of *pin1-613*. We tested two independent PIN1b events for
331 complementation of *pin1-613* when combined with a SoPIN1 event that showed partial

332 complementation, but all double SoPIN1/PIN1b expressing *pin1-613* plants appeared
333 phenotypically similar to the SoPIN1-only complementation (data not shown). Thus
334 SoPIN1 combined with PIN1b is no better than SoPIN1 alone. In total, these results
335 demonstrate that when expressed in *Arabidopsis,* there is a clear functional separation
336 between SoPIN1 and PIN1b independent of transcriptional control.

337

## 338 SoPIN1 and PIN1b show different behaviors when expressed in the 339 meristem epidermis

340 Epidermal-specific AtPIN1 expression is sufficient to rescue organ initiation in *atpin1*
341 mutants (Bilsborough et al., 2011), highlighting the importance of AtPIN1 epidermal
342 expression to organ initiation. We wanted to test specifically the ability of SoPIN1 and
343 PIN1b to perform this epidermal function. In order to drive increased PIN1b expression
344 in the epidermis, and to help reduce transgene position-effect variation of expression
345 level, we utilized a two-component expression system in the Landsberg *erecta* (L*er*)
346 background to drive SoPIN1 and PIN1b under the control of the epidermis-enriched
347 Arabidopsis ML1 promoter (Hereafter designated *proAtML1*>>) (Lenhard and Laux,
348 2003; Sessions et al., 2002). Under the control of *proAtML1* we achieved consistently
349 high epidermal accumulation of both SoPIN1 and PIN1b, but similar to the *proAtPIN1*
350 driven expression described above, only SoPIN1 showed clear convergent polarization
351 patterns around the sites of organ initiation (Figure 6A-6D, Figure 6 supplement 1 and
352 2) (11 of 11 meristems). Despite consistently high epidermal expression with this
353 system, PIN1b polarity remained difficult to determine, and in many cells the abundance

354 of protein on the membrane remained low (Figure 6D) (13 of 13 meristems). Instead,
355 PIN1b accumulated in intracellular bodies, especially in the cells of the apical dome and
356 the central domain of initiating organs (Figure 6 – supplement 3 panels A-D).
357 Intracellular PIN1b did not co-localize with early endosomes as assayed by FM4-64
358 (Figure 6 – supplement 3 panel C arrows), or show the perinuclear localization
359 characteristic of the endoplasmic reticulum, suggesting accumulation in either the golgi
360 apparatus or in vacuoles. PIN1b abundance and polarity was highest at the boundaries
361 of lateral organs (Figure 6 - supplement 2). Thus SoPIN1 and PIN1b show consistent
362 behaviors in the meristem epidermis when expressed under either *proAtPIN1* or
363 *proAtML1.* Despite increased PIN1b expression under *proAtML1,* and a resulting
364 increase in protein accumulation in the apex, PIN1b was still unable to form convergent
365 polarization patterns in wild-type plants.

366

## 367 Both SoPIN1 and PIN1b can rescue the Arabidopsis *pin1-4* mutation 368 when expressed in the meristem epidermis

369 In order to determine whether the increased PIN1b abundance in the epidermis
370 achieved by the *proAtML1* two-component system had functional consequences, we
371 crossed these transgenes to the *pin1-4* mutant allele. The *pin1-4* allele is in the
372 Landsberg *erecta* (L*er*) background and has a single P579 to L amino acid change in
373 the second-to-last transmembrane domain of AtPIN1 (Bennett et al., 1995), but the
374 phenotype is similarly severe to the null *pin1-613* allele (Figure 7A-C). However, using
375 immuno-localization we detected abundant AtPIN1 protein produced in *pin1-4*

376 meristems (Figure 7C), while similar to previous authors, we did not detect any protein
377 in pin meristems of the null *pin1-613* allele (Figure 7B) (Absmanner et al., 2014; Bennett
378 et al., 2006) (6 *pin1-613* meristems, 5 *pin1-4* meristems). The AtPIN1 protein detected
379 in *pin1-4* mutants accumulated primarily in the provascular tissues below the pin apex
380 (Figure 7C), and appeared apolar (Figure 7D). Instead, the perinuclear AtPIN1
381 localization in *pin1-4* suggests accumulation in the endoplasmic reticulum (Figure 7D,
382 arrow). The presence of AtPIN1 protein produced in *pin1-4* mutants indicates that
383 *AtPIN1* in this background may retain partial function despite the severity of the mutant
384 phenotype.

385 Indeed, both SoPIN1 and PIN1b driven by *proAtML1* were able to rescue the organ
386 formation defects of *pin1-4* (Figure 8A). In contrast to the partial SoPIN1-mediated
387 complementation and failure of PIN1b to complement *pin1-613* described above, both
388 SoPIN1 and PIN1b-complemented *pin1-4* plants made WT flowers that produced seed
389 (Figure 8 – supplement 1). In addition, SoPIN1 and PIN1b were both able to rescue bulk
390 auxin transport in the *pin1-4* basal internode, although PIN1b was less effective than
391 SoPIN1 (Figure 8B). In general SoPIN1 and PIN1b-mediated complementation of *pin1-4*
392 was phenotypically similar, but perhaps as a result of the decreased transport rate in
393 PIN1b-complemented *pin1-4* plants, this genotype showed a significant increase in
394 stem diameter (Figure 8C), providing further evidence that SoPIN1 and PIN1b are not
395 functionally equal.

396 SoPIN1-complemented *pin1-4* meristems were slightly smaller than wild-type (Figure 6
397 – supplement 1), but the protein localization was similar to the pattern observed in the
398 WT background, with clear convergent polarization around initiating organs (Figure 6E,

399 6G) (10 of 10 meristems). In contrast, compared to the WT background, PIN1b
400 localization in *pin1-4* was dramatically altered (compare Figure 6B with Figure 6F). Most
401 obvious was an increase in membrane targeted PIN1b and a corresponding reduction in
402 intracellular PIN1b (Figure 6H, Figure 6 supplement 3 panels E-H). PIN1b polarization
403 in the *pin1-4* background was more apparent than in wild-type, and convergent
404 polarization patterns clearly marked incipient organs (Figure 6H) (10 of 10 meristems).
405 PIN1b-complemented meristems accumulated less PIN protein in the apical dome
406 compared to SoPIN1-complemented meristems, and the meristems were larger (Figure
407 6 – supplement 2).

408 In the basal internode, both PINs had similar accumulation patterns in the cortex (co)
409 and epidermis layers (Figure 6I-J arrows), and both showed rootward polarization in the
410 epidermis (Figure 6K-L arrows). Despite this expression domain being drastically
411 different than the wild-type vascular-associated pattern of AtPIN1 (Bennett et al., 2006;
412 Gälweiler et al., 1998), expression in these few cortex layers and epidermis was
413 apparently sufficient to drive near wild-type levels of rootward bulk auxin transport in
414 *pin1-4* (Figure 8B). Thus, while both proteins can complement the *pin1-4* organ initiation
415 phenotype, the SoPIN1 and PIN1b complemented lines have differing localization
416 patterns, slightly different auxin transport properties, and minor differences in meristem
417 and mature plant morphologies, suggesting once again that SoPIN1 and PIN1b are not
418 functionally identical.

419

420

421 # Discussion

422 ## The SoPIN1 and PIN1 clades have different functions in
423 Brachypodium

424 During spikelet development in Brachypodium, SoPIN1 forms convergent polarization
425 patterns surrounding the sites of organ initiation and strong expression of the auxin
426 response reporter DR5 (O'Connor et al., 2014). We provide additional evidence here
427 that SoPIN1 polarizes towards sites of high auxin concentration by showing that a DII
428 minimum occurs at SoPIN1 convergence points. In *sopin1* mutants the reduction of DII
429 does not occur, suggesting that SoPIN1 functions to concentrate auxin at epidermal
430 maxima, and similar to Arabidopsis, this is required for organ initiation in the
431 inflorescence. The barren inflorescence phenotype of *sopin1-1* mutants, and the
432 specificity of SoPIN1 for the outer tissues and for convergent polarization patterns in
433 Brachypodium provides further support for the idea that auxin maximum formation is
434 necessary for organ initiation, and that this is primarily mediated by convergent PIN in
435 the meristem epidermis (Bhatia et al., 2016; Jönsson et al., 2006; Kierzkowski et al.,
436 2013; Smith et al., 2006).

437 SoPIN1 clade mutants have been reported in the legume *Medicago truncatula* and in
438 tomato (*Solanum lycopersicum*), and these mutants show pleiotropic phenotypes
439 involving phyllotaxy, organ initiation, inflorescence branching, leaf serrations, and leaf
440 compounding, but they do not form barren pin meristems (Martinez et al., 2016; Zhou et
441 al., 2011). These wider morphogenetic events also involve epidermal PIN convergence
442 points and associated auxin maxima (Barkoulas et al., 2008; Bilsborough et al., 2011),

443 suggesting a general role for SoPIN1 clade members in generating such maxima. The
444 lack of barren pin-formed meristems in these mutants suggests that different species
445 are variably dependent on SoPIN1-generated auxin maxima for organ initiation. Even in
446 Brachypodium and Arabidopsis, barren meristems in *sopin1* and at*pin1* respectively are
447 restricted to later stages of development, so organs are able to form in the absence of
448 SoPIN1 or AtPIN1 function.

449 In contrast to *sopin1* mutants, loss of *pin1* clade function in Brachypodium has very little
450 effect on organ initiation, despite both PIN1a and PIN1b being expressed and polarized
451 away from auxin maxima in developing organs (O'Connor et al., 2014). Auxin drainage
452 is thought necessary for proper organ size and placement (Bhatia et al., 2016; Deb et
453 al., 2015), but the most evident phenotype in *pin1a/pin1b* mutants is the alteration of
454 internode length. The increased internode length in *pin1b,* and severely reduced
455 internode length in *pin1a/pin1b* double mutants, provides new genetic tractability to
456 address how PINs regulate tissue growth in the shoot independent of organ initiation, a
457 PIN function that is experimentally inaccessible in Arabidopsis because of the initiation
458 defects of *atpin1* mutants.

459 Grasses contain intercalary meristems, bands of indeterminate tissue separated from
460 the apical meristem that are responsible for internode growth after organ initiation.
461 Auxin dynamics in this more basal meristematic tissue may be important for controlling
462 stem growth. Indeed**,** loss of the ABCB1 auxin exporter in maize and Sorghum results in
463 dwarfism associated with reduced activity of intercalary meristems (Knöller et al., 2010;
464 Multani et al., 2003). The role of PIN1a and PIN1b in regulating intercalary meristem

465 growth will be an important avenue for future work, especially since plant stature has
466 played such an important role in grass domestication.

467

## 468 The properties that define PIN behavior and function

469 **Membrane accumulation.** We used heterologous expression of SoPIN1 and PIN1b in
470 Arabidopsis to explore the ways in which different PIN family members may have
471 different properties post-transcription (Summarized in Figure 9). When expressed in the
472 meristem epidermis in wild-type Arabidopsis, SoPIN1 is localized to the membrane in
473 most cells while PIN1b often accumulates internally (Figure 6 - supplement 3). Thus,
474 with the same transcriptional control, different PINs can vary in the degree to which,
475 after protein production, they accumulate at the plasma membrane. The differential
476 membrane targeting of PIN1b and SoPIN1 is a tissue-specific phenomenon however,
477 because unlike in the epidermis, in the basal internode both PINs accumulate at the
478 rootward plasma membrane (Figure 3 - supplement 1 panels E and F). The regulation
479 of PIN plasma membrane polar targeting and endocytic recycling has been an important
480 avenue for understanding PIN function and general membrane protein biology
481 (Luschnig and Vert, 2014). Our results provide further evidence that at least some of the
482 signals governing membrane accumulation are inherent in, and vary between, different
483 PIN family members (Wisniewska et al., 2006).

484 **Tissue accumulation.** Under the same transcriptional control AtPIN1, SoPIN1, and
485 PIN1b show different tissue-level accumulation patterns in Arabidopsis. In wild-type
486 plants, *proAtPIN1*-expressed PIN1b shows reduced overall accumulation in the

487 epidermis compared to AtPIN1 or SoPIN1 (Compare Figure 3D-3F). Even with greater
488 expression under *proAtML1,* the intracellular PIN1b signal observed in the meristem
489 epidermis (Figure 6 - supplement 3) suggests that PIN1b protein could be actively
490 targeted to the vacuole for degradation as has been shown for PIN2 in the root (Abas et
491 al., 2006; Kleine-Vehn et al., 2008b). In contrast, SoPIN1 is abundant in the meristem
492 epidermis and accumulates in the mature cortex and pith tissues where AtPIN1 and
493 PIN1b do not (Figure 3H arrows). Because we observed clear AtPIN1 accumulation in
494 the immature pith (Figure 3 - supplement 1 panel D), this suggests that *proAtPIN1* is at
495 least initially active in pith tissue and that the PIN1 clade members, AtPIN1 and PIN1b,
496 are removed later in development, while SoPIN1 is not. Laser capture micro-dissection
497 and RNAseq of mature stem tissue has detected abundant *AtPIN1* transcription in the
498 mature pith (T. Greb, personal communication, February 2017), suggesting that even at
499 maturity AtPIN1, and probably PIN1b are actively cleared post-transcriptionally from this
500 tissue. Our results suggest that the AtPIN1 expression domain is far broader than is
501 indicated by the protein accumulation pattern, and further highlight the importance of
502 PIN post-transcriptional regulation for controlling PIN tissue-level abundance.

503 In Arabidopsis, endogenous PIN family members show a degree of cross-regulation
504 where loss-of-function mutations in one PIN family member result in tissue-level
505 accumulation of a different PIN in a compensatory pattern (Blilou et al., 2005; Paponov
506 et al., 2005; Vieten et al., 2005). We observed similar behavior in the *pin1-613* null
507 background, where SoPIN1 and PIN1b accumulation in the meristem epidermis was
508 increased in the absence of AtPIN1 (Figure 5 supplements 1 and 2). This sensitivity of
509 SoPIN1 and PIN1b to the presence of AtPIN1, even while under the *AtPIN1* promoter,

510 suggests that wild-type AtPIN1 is able to compete with SoPIN1 and PIN1b post-
511 transcriptionally for residency at the membrane. However, we did not observe the same
512 competitive effect with *proAtML1* where SoPIN1 and PIN1b tissue-level accumulation,
513 though not membrane residence, seemed similar between *pin1-4* mutant and wild-type
514 meristems (Figure 6 - supplements 1 and 2). This difference between *proAtPIN1* and
515 *proAtML1* may be because PIN transcription under *proAtPIN1* is sensitive to the dosage
516 of other PINs as has been suggested (Vieten et al., 2005). Alternatively, the lack of
517 increased SoPIN1 and PIN1b accumulation in the *pin1-4* mutant background may be
518 because the AtPIN1 protein produced in *pin1-4* is still able to compete with the other
519 expressed PINs. Regardless, these results highlight the sensitivity of PIN tissue-level
520 abundance to both transcriptional and post-transcriptional control, and the variability
521 between PIN family members independent of transcription.

522 **Transport activity.** In Arabidopsis, phosphorylation of PINs by several different families
523 of protein kinases is thought necessary for efficient auxin transport (Absmanner et al.,
524 2014; Barbosa et al., 2014; Jia et al., 2016; Willige et al., 2013). PIN activation by
525 phosphorylation may explain the inability of PIN1b to mediate bulk auxin transport in the
526 basal internode of *pin1-613* plants despite being expressed, accumulating at the
527 membrane, and being polarized rootward in this tissue (Figure 4D, Figure 5M). It is
528 possible that in the *proAtPIN1* domain PIN1b does not interact with the appropriate
529 activating kinase, and it is thus unphosphorylated and inactive. Indeed, a partially
530 unphosphorylatable form of AtPIN1 fails to complement fully the bulk auxin transport
531 defect of *pin1-613* mutants in the basal internode (Absmanner et al., 2014), and AtPIN1

532 polarity can be uncoupled from phosphorylation status, and thus presumably transport
533 activity can be independent of polarization (Weller et al., 2017).

534 However, when expressed using *proAtML1,* PIN1b expression in the outer tissue layers
535 of the basal internode appears sufficient to mediate bulk auxin transport in *pin1-4*
536 (Figure 8B). One explanation for this is that PIN1b activity may be tissue dependent,
537 perhaps because of the differing expression domains of activating kinases (Absmanner
538 et al., 2014). Arabidopsis PIN4 and PIN7 are present in the *proAtML1* domain (Bennett
539 et al., 2016), making it conceivable that these PINs are the normal targets of activating
540 kinases in this tissue. Alternatively, kinases in the L*er* genetic background may be more
541 effective at activating PIN1b than those in Col, but the dramatic effect of the *pin1-4*
542 allele vs wild-type *AtPIN1* on PIN1b polarization behavior within the L*er* background
543 makes this explanation unlikely (see below). In either case, the behavior of PIN1b in
544 *pin1-613* provides a clear indication that even once a PIN has accumulated at the cell
545 membrane in a tissue it may not be active.

546 **Interaction.** A particularly striking result is the ability of PIN1b to form convergent
547 polarization patterns and mediate organ initiation in the *pin1-4* missense mutant
548 background when it is unable to do so in the null *pin1-613* background. It is unlikely that
549 differences between *proAtPIN1* and *proAtML1*-mediated expression can explain this
550 differential complementation because both promoters drive expression in the epidermis,
551 and both promoters are sufficient to complement *atpin1* mutants using wild-type AtPIN1
552 as well as SoPIN1. As described above, it is possible that differences in activating
553 enzymes or similar interactors between the L*er* and Col backgrounds could contribute to
554 the strikingly different behavior of PIN1b in *pin1-4* vs *pin1-613*. Indeed, mutation of the

555 leucine-rich repeat receptor-like kinase *ERECTA,* which is mutated in the L*er*
556 background, has known effects on PIN1 localization when combined with other
557 mutations in the *ERECTA* family (Chen et al., 2013; Torii et al., 1996). However, the
558 dramatic effect of wild-type AtPIN1 vs *pin1-4* on PIN1b membrane targeting (compare
559 Figure 6 - supplement 3 panels A-D to E-H) within the L*er* background suggests the
560 differing genetic backgrounds of each complementation (L*er* vs Col-0) is not sufficient to
561 explain the differential complementation.

562 Instead, the strong influence of *pin1-4* on PIN1b membrane targeting and polarity in the
563 meristem epidermis suggests that PIN1b may be cooperating with a partially functional
564 *pin1-4* protein and together they recapitulate the organ initiation functions of wild-type
565 AtPIN1. PIN1b interaction with *pin1-4* in the outer cortex of the stem may also explain
566 the ability of PIN1b to rescue bulk transport in the basal internodes of *pin1-4* mutants
567 while it cannot in the null *pin1-613* allele. Partial *pin1-4* function is further supported by
568 the result that SoPIN1 complementation of the null *pin1-613* allele is incomplete, and
569 because of flower defects the plants are sterile (Figure 4C), while SoPIN1-mediated
570 complementation of *pin1-4* is complete, and flowers are phenotypically normal and set
571 seed (Figure 8 - supplement 1). Accordingly, SoPIN1 convergent polarization patterns
572 are more evident in the presence of *pin1-4* than they are during complementation of the
573 null *pin1-613* allele (Compare 5A and 6E), further evidence that residual *pin1-4* function
574 augments SoPIN1 during *pin1-4* complementation. Combined, these data suggest that
575 the *pin1-4* allele is hypomorphic, and that it provides some necessary function to PIN1b.

576 If PIN1b is indeed inactive in null *pin1-613* mutants as we hypothesized above, then it is
577 possible *pin1-4* facilitates the interaction of PIN1b with the appropriate activating kinase,

578 and this allows PIN1b to perform organ initiation and bulk transport. Alternatively,
579 interaction between PIN1b and *pin1-4* may facilitate proper membrane targeting or
580 polarization of either protein, resulting in functional transport. The increased level of
581 polar, plasma-membrane localized PIN1b in *pin1-4* meristems supports the idea that
582 *pin1-4* controls PIN1b membrane residency, but it cannot explain why PIN1b appears
583 unable to mediate bulk transport in *pin1-613* despite being membrane-localized and
584 polar in the basal internode.

585 Direct PIN-PIN interactions have so far not been shown, but if one PIN type can convey
586 targeting, polarity, or activity information to another through direct or indirect interaction,
587 this may be relevant to auxin transport in tissues where multiple PINs are coexpressed,
588 such as in the Arabidopsis root meristem (Blilou et al., 2005), or in the shoot apical
589 meristems of most angiosperms where the SoPIN1 and PIN1 clade proteins likely
590 overlap, as they do during spikelet development in Brachypodium (O'Connor et al.,
591 2014).

592 **Polarity.** We previously showed that the polarization dynamics of SoPIN1, PIN1a, and
593 PIN1b in *Brachypodium* could be modeled by assigning two different polarization modes
594 to the SoPIN1 and PIN1 clades (O'Connor et al., 2014). In the model, SoPIN1 orients
595 toward the adjacent cell with the highest auxin concentration, thus transporting auxin up
596 the concentration gradient and providing a positive feedback to concentrate auxin into
597 local maxima. In contrast, in the model, PIN1a and PIN1b proteins are allocated in
598 proportion to net auxin flux, thus providing a positive feedback in which flux through the
599 tissue is amplified by the allocation of PIN1a/b in the direction of that flux. The
600 assignment of two different polarization modes was previously used to describe the

601 behavior of AtPIN1 during organ placement and vein patterning using an auxin-
602 concentration based switching mechanism between the up-the-gradient (UTG) and with-
603 the-flux (WTF) polarization modes (Bayer et al., 2009). However, it has also been
604 suggested that a flux-based mechanism alone can account for both convergence points
605 and vein patterning (Abley et al., 2016; Stoma et al., 2008).

606 Despite evidence that convergent PIN polarization is dependent on localized auxin
607 signaling in adjacent cells (Bhatia et al., 2016), there are still no proven mechanisms for
608 direct sensing of intercellular auxin gradients or auxin fluxes across membranes. The
609 *sopin1, pin1a,* and *pin1b* phenotypes in Brachypodium are consistent with different
610 polarization modes. SoPIN1 is required for organ initiation and the formation of auxin
611 maxima in Brachypodium, which is primarily modeled using UTG polarization (Bayer et
612 al., 2009; Jönsson et al., 2006; Smith et al., 2006). On the other hand, *pin1a* and *pin1b*
613 mutant plants do not show organ initiation defects, but rather only have internode
614 elongation defects, a tissue where WTF models have been used to explain PIN
615 dynamics and measured auxin transport kinetics during vein patterning and the
616 regulation of branch outgrowth (Bayer et al., 2009; Bennett et al., 2016; Mitchison,
617 1980; Mitchison et al., 1981; Prusinkiewicz et al., 2009).

618 In wild-type Brachypodium, the SoPIN1 and PIN1a/b expression domains are almost
619 entirely mutually exclusive (O'Connor et al., 2014), making it possible that the observed
620 polarization differences between the two clades are due to expression context or tissue-
621 level stability, and not to functional differences between the proteins themselves. More
622 specifically, perhaps an UTG mechanism dominates the epidermis while a WTF
623 mechanism is utilized in the internal tissues, and different PINs interact equally with

624 these context-dependent mechanisms. Our heterologous expression studies do not
625 exclusively support context-dependent or protein-dependent mechanisms for SoPIN1
626 and PIN1 polarization. It is clear that alone only SoPIN1 and AtPIN1 show the
627 convergent polarization patterns associated with UTG polarization, and alone only
628 SoPIN1 and AtPIN1 are thus able to mediate organ initiation, while PIN1b cannot. On
629 the other hand, all three PINs are capable of rootward polarization in the basal
630 internode tissue, and PIN1b can be co-opted to convergent polarization at the meristem
631 epidermis in the presence of *pin1-4*. The results presented here do not demonstrate
632 whether within a single cell SoPIN1 and PIN1b would orient differently with respect to
633 auxin as might be expected for the dual polarization model (O'Connor et al., 2014).
634 However, such context-independent polarization behavior was previously observed for
635 PIN1 and PIN2 in the root where both PINs can polarize in opposing directions within a
636 single cell type when expressed in the PIN2 domain (Kleine-Vehn et al., 2008a;
637 Wisniewska et al., 2006).

638 **Outlook**

639 In total, our Brachypodium mutant phenotypes and heterologous expression results
640 point to multiple levels at which PIN family members can be functionally distinct.
641 Differential membrane targeting, tissue level accumulation, transport activity, indirect or
642 direct interaction, and the resultant polarity may all contribute to the dynamics of PIN
643 action during plant development. In most flowering plants two PIN clades, SoPIN1 and
644 PIN1, with differing functions and differing transcriptional and post-transcriptional
645 properties mediate auxin transport in the shoot, but these properties are seemingly
646 combined into AtPIN1 in Arabidopsis and other Brassicaceae species. Because PIN1b

647 alone is unable to mediate organ initiation while AtPIN1 can, and these two PINs are
648 both members of the same clade, AtPIN1 may have gained the ability to form
649 convergent polarization patterns and mediate organ initiation after, or coincident with,
650 the loss of the SoPIN1 clade. Indeed, when comparing Brassicaceae PIN1 proteins
651 against a broad sampling of other angiosperm PIN1 proteins, the Brassicaceae PIN1
652 proteins have several divergent protein domains (Figure 9 - supplement 1), suggesting
653 possible neofunctionalization within the Brassicacea family. Alternatively, an expansion
654 of the PIN3,4,7 clade is also characteristic of Brassicacea species (Bennett et al., 2014;
655 O'Connor et al., 2014), making it possible duplicated members of this clade buffered the
656 loss of SoPIN1. However, there is no indication that PIN3,4,7 have a role in organ
657 initiation in the inflorescence (Guenot et al., 2012). Regardless, we believe the
658 combination of SoPIN1 and PIN1 characteristics into AtPIN1 coincident with the loss of
659 the SoPIN1 clade represents a form of reverse-subfunctionalization, the combination of
660 functions originally split between homologs into a single protein after gene loss. It is not
661 surprising that PINs may be particularly amenable to this kind of functional evolution
662 because, as described above, there are several post-transcriptional regulatory steps
663 that ultimately combine to control PIN function in plants. The output of auxin transport is
664 the sum of an extensive network of post-transcriptional interactions that all act to
665 regulate auxin transport itself, and this gives the system plasticity during development,
666 and perhaps also over evolutionary time.

667

668

669 # Materials and Methods

670 ## *sopin1-1*, *pin1a-1,* and *pin1b-1* creation with CRISPR

671 SoPIN1 (Bradi4g26300), PIN1a (Bradi1g45020), and PIN1b (Bradi3g59520) were
672 targeted with CRISPR using vectors developed for rice (Miao et al., 2013). CRISPR
673 constructs were transformed into Brachypodium inbred line Bd21-3 using previously
674 published methods (Bragg et al., 2015).

675 *sopin1-1* CRISPR

676 The SoPIN1 guide was AGGCTGTCGTACGAGGAGT. This guide was shorter than the
677 typical 20bp in an effort to provide greater target specificity for SoPIN1 (Fu et al., 2014).
678 In the T0 regenerated plants, 5 out of 9 independent transgenic events showed severe
679 organ initiation defects, and all 5 contained lesions in the SoPIN1 CRIPSR target site.
680 Unfortunately, only one of the events with a T0 phenotype set seed. In the T1 progeny
681 of this event only those individuals that contained the CRISPR transgene showed
682 lesions in the SoPIN1 CRISPR target site, and these plants showed the *sopin1*
683 phenotype and thus failed to set seed, suggesting active editing by the SoPIN1 CRISPR
684 transgene in this event.

685 Not all events showed such efficient editing however, and we identified an independent
686 T1 family where a C insertion in the SoPIN1 CRISPR target site co-segregated with the
687 barren inflorescence phenotype. We designated this allele, which causes a premature
688 stop codon before the end of the third exon codon 739 base pairs downstream from the
689 target site, *sopin1-1*. (Primer IDs 1-2 Table 1) We backcrossed a heterozygous *sopin1-1*

690 plant to the Bd21-3 parental line and all F1 progeny (N=4) were wild-type. In the F2
691 generation, plants homozygous for the *sopin1-1* lesion co-segregated with the barren
692 inflorescence phenotype (N=60: 32 het, 18 homo,10 wt). Amongst these plants, 16 did
693 not have the Cas9 transgene (Primer IDs 3-4 Table 1), and the barren inflorescence
694 phenotype still co-segregated with the *sopin1-1* lesion (N=16: 8 het, 3 homo, 5 wt). We
695 crossed the T1 *sopin1-1* heterozygous plant with a line homozygous for the previously
696 published SoPIN1-CITRINE genomic reporter line (O'Connor et al., 2014). In the F2 we
697 identified families homozygous for *sopin1-1* but segregating for the SoPIN1-CITRINE
698 transgene. Only individuals that lacked the SoPIN1-CITRINE transgene showed a
699 *sopin1-1* phenotype, while those that contained the SoPIN1-CITRINE transgene made
700 spikelets and set seed (Figure 1 - supplement 1). This complementation was
701 independent of the presence of Cas9.

702 *pin1a-1* CRISPR

703 The PIN1a guide was ATCTACTCCCGGCGGTCCAT. We identified edited plants in the
704 T1 generation (Primer IDs 5-6 Table 1), then found a homozygous T insertion in the T2
705 generation which was independent of Cas9, resulting in a premature stop codon 939
706 base pairs downstream, here designated *pin1a-1*. No single-mutant *pin1a-1* phenotypes
707 were observed.

708 *pin1b-1* CRISPR

709 The PIN1b guide was AGGGCAAGTACCAGATCC. We identified a single plant from
710 the regenerating T0 PIN1b CRISPR population that had longer basal internodes and
711 twisted leaves. This plant was homozygous for an A deletion in the PIN1b CRISPR

712 target site causing a premature stop in the second exon 502 base pairs downstream,
713 here designated *pin1b-1* (Primer IDs 7-8 Table 1). All T1 progeny showed the *pin1b*
714 phenotype and were homozygous for the *pin1b-1* lesion. We backcrossed these T1
715 plants to Bd21-3 and all F1 progeny had a wild-type phenotype (N=11). In the F2, the
716 *pin1b* phenotype co-segregated with the *pin1b-1* lesion (N= 215, 91 het, 39 homo, 26
717 wt). Amongst these plants, 24 did not have the Cas9 transgene, and the *pin1b*
718 phenotype still co-segregated perfectly with the *pin1b-1* lesion (N=24: 10 het, 6 homo, 8
719 wt). We crossed *pin1b-1* without Cas9 to a line homozygous for the previously
720 published PIN1b-CITRINE transgene (O'Connor et al., 2014). In the F3 we identified
721 lines homozygous for both the transgene and *pin1b-1* and used these to quantify
722 internode lengths compared to *pin1b-1* (Figure 2 - supplement 1).

723 *pin1a-1 / pin1b-1* double mutant.

724 Homozygous *pin1b-1* lacking Cas9 was crossed to homozygous *pin1a-1* lacking Cas9.
725 In the F2 phenotypically *pin1b-1* plants that were also genotyped heterozygous for
726 *pin1a-1* were identified. In the homozygous *pin1b-1* F3 generation the double *pin1a-1 /*
727 *pin1b-1* mutant phenotype segregated perfectly with the *pin1a-1* lesion (N=2: 10 het, 5
728 homo, 8 wt). Double *pin1a-1 / pin1b-1* mutants were easily identified by phenotype and
729 produce seed.

## 730 Brachypodium Reporter Constructs

731 All constructs were cloned using Multi-site Gateway (Invitrogen) and were transformed
732 into Brachypodium Bd21-3 using previously published methods (Bragg et al., 2015). For
733 pZmUbi::DII-Venus, we first cloned the maize ubiquitin promoter into pDONR P4-P1R

734 (Primer IDs 9-10 Table 1) and this was subsequently recombined with pDONR 221
735 containing Arabidopsis DII and pDONR P2R-P3 containing VENUS-N7 (Brunoud et al.,
736 2012) into the Multi-site Gateway binary vector pH7m34GW
737 (http://gateway.psb.ugent.be/). In the T3 generation, degradation of DII-Venus in the
738 presence of auxin was validated by treating excised Brachypodium spikelet meristems
739 with 1 μM 1-naphthaleneacetic acid (NAA) or mock treatment in 70% ethanol, and
740 imaging every 30 min (Figure 1 –supplement 2).

741 For SoPIN1-Cerulean, the promoter plus 5' coding pDONR-P4-P1R and 3' coding plus
742 downstream pDONR-P2R-P3 fragments from (O'Connor et al., 2014) were used. Maize
743 codon-optimized Cerulean florescent protein, courtesy of David Jackson, was amplified
744 with 5x Ala linkers and cloned into pENTR/D-TOPO. These three fragments were then
745 recombined into pH7m34GW.

## 746 Arabidopsis Reporter Constructs

747 All constructs were cloned using Multi-site Gateway (Invitrogen) and transformed using
748 standard floral dip. For *proAtPIN1* complementation, a 3.5kb Arabidopsis PIN1 promoter
749 region was amplified from a genomic clone previously reported to complement the *pin1*
750 (Heisler et al., 2005) and cloned into Gateway vector pDONR P4-P1R (Primer IDs 11-
751 12 Table 1). For each Brachypodium PIN-CITRINE fusion construct, the entire PIN
752 coding region, including the CITRINE insertion, was amplified from the previously
753 published reporter constructs (O'Connor et al., 2014) and cloned into pENTR /D-TOPO
754 (Primer IDs 13-16 Table 1). The CITRINE fusion in each is located in a position known
755 to complement *pin1* mutations (Heisler et al., 2010; Wisniewska et al., 2006; Xu et al.,

756 2006). The *proAtPIN1* pDONR P4-P1R and PIN coding region pENTR/D-TOPO vectors
757 were then recombined into Gateway binary vector pH7m24GW
758 (http://gateway.psb.ugent.be/) and transformed by floral dip into both Col-0 and plants
759 heterozygous for *pin1-613* (also known as *pin1-7,* SALK_047613) (Bennett et al., 2006;
760 Smith et al., 2006). Complementation was assessed in the T3 generation, and all plants
761 were genotyped for both the *pin1-613* mutation (Primer IDs 17-19 Table 1) and for
762 presence of the PIN transgene (Primer IDs 20-22 Table 1).

763 For the *proAtML1* lines the PIN coding regions with CITRINE insertion pENTR /D-TOPO
764 Gateway vectors were recombined downstream of the two-component OP promoter in
765 vector pMoA34-OP (Moore et al., 1998) and then transformed into the *proAtML1* driver
766 line in the Landsberg *erecta* background (Lenhard and Laux, 2003). Lines homozygous
767 for both the *proAtML1* driver and OP::PIN were crossed to het *pin1-4* and
768 complementation was assessed in the F2 and F3 generations. All complemented plants
769 were genotyped for *pin1-4* (Primer IDs 23-24 Table 1), the Brachypodium PINs (Primer
770 IDs 20-22 Table 1), and the presence of the ML1 driver transgene (Primer IDs 25-26
771 Table 1).

## 772 Confocal and Scanning Electron Microscopy

773 All confocal images were captured on a Zeiss 780 laser scanning confocal using a W
774 Plan-Apochromat 20x or 63x magnification 1.0 numerical aperture objectives. Detection
775 wavelengths: 517-570nm for CITRINE-tagged PINs, 535-552 for DII-Vinus, 463-509 for
776 SoPIN1-CERULEAN, 490-543 for AtPIN1-GFP, 691-753nm for FM4-64, 561-606nm for
777 Dylight 549, 631-717nm for Propidium Iodide, and 646-726 for chlorophyll A auto-

778 fluorescence. The pinhole was set to 1 airy unit for all meristem stacks and details of
779 sub-epidermal polarization, but was open to the maximum setting for tiled longitudinal
780 and cross sections of the basal internode (Figures 3D-L, 5C-H and 6I-J). Detection gain
781 and laser power were varied according to signal strength unless direct comparisons
782 between genotypes were made as indicated in figure legends.

783 Cryo scanning electron microscopy was performed on a Zeiss EVO HD15 SEM fitted
784 with a LaB6 filament and a Quorum PP3010T (Quorum Technololgies, Lewes, Sussex.
785 UK) cryo preparation unit using the BSD (Backscattered electron) detector with probe
786 current as set to 10 nA, and 15.00 kV gun voltage. Frozen samples were coated in
787 <1.5nm Pt.

## 788 Auxin Transport Assays

789 Auxin transport assays were carried out as described in (Crawford et al., 2010). Briefly,
790 17 mm long basal internodes were excised and the apical end submerged in 30 µl
791 Arabidopsis salts (ATS) without sucrose (pH = 5.6) containing 1 µM $^{14}$C-IAA (American
792 Radiolabeled Chemicals). After 6 hours incubation, the basal 5 mm segment was
793 excised, cut in half, and shaken overnight at 400 RPM in 200 µl scintillation liquid prior
794 to scintillation counting. 10µM N-1-Naphthylphthalamic Acid (NPA), an auxin transport
795 inhibitor, was added prior to incubation for negative controls.

## 796 AtPIN1 Immuno-Localization

797 Detection of AtPIN1 in sectioned apexes was performed as previously described
798 (O'Connor et al., 2014). Commercial polyclonal goat anti-AtPIN1 (AP-20) was used at a

799 concentration of 1:150 (Santa Cruz Biotechnology). Affinity-purified Donkey Anti-Goat
800 Dylight 549 secondary was used at a concentration of 1:200 (Jackson Immuno
801 Research). Control samples where the primary antibody was omitted showed a similar
802 level of background signal as *pin1-613* null mutant samples.

803

## 804 Acknowledgments

805 Thanks to Raymond Wightman for SEM assistance, Martin van Rongen for assistance
806 with transport assays and *pin1-613* oligos, Tom Bennett for *proAtPIN1* oligos, Marcus
807 Heisler for AtPIN1-GFP construct and *pin1-4* genotyping assistance, Teva Vernoux for
808 DII plasmids, David Jackson for maize codon-optimized Cerulean, and to all the
809 members of the Leyser lab. Thanks also to Graeme Mitchison, Katie Abley, Michael
810 Raissig, and Pau Formosa-Jordan for helpful comments on the manuscript.

811

## 812 Competing interests

813 The authors have no competing interests.

814

## 815 References

816 **Abas, L., Benjamins, R., Malenica, N., Paciorek, T., Wisniewska, J.,**
817 **Wirniewska, J., Moulinier-Anzola, J. C., Sieberer, T., Friml, J. and**
818 **Luschnig, C.** (2006). Intracellular trafficking and proteolysis of the
819 Arabidopsis auxin-efflux facilitator PIN2 are involved in root gravitropism. *Nat*

820 *Cell Biol* **8**, 249–256.

821 **Abley, K., Marée, A. F. and Coen, E.** (2016). Formation of polarity
822 convergences underlying shoot outgrowths. *eLife* **5**, 2061.

823 **Absmanner, B., Barbosa, I. C. R., Willige, B. C., Fastner, A., Streit, V., Port,**
824 **S. A. and la Fuente van Bentem, de, S.** (2014). Auxin efflux by PIN-
825 FORMED proteins is activated by two different protein kinases, D6 PROTEIN
826 KINASE and PINOID. *eLife* **3**.

827 **Adamowski, M. and Friml, J.** (2015). PIN-Dependent Auxin Transport: Action,
828 Regulation, and Evolution. *The Plant Cell* **27**, 20–32.

829 **Barbosa, I. C. R., Zourelidou, M., Willige, B. C., Weller, B. and**
830 **Schwechheimer, C.** (2014). D6 PROTEIN KINASE activates auxin transport-
831 dependent growth and PIN-FORMED phosphorylation at the plasma
832 membrane. *Dev Cell* **29**, 674–685.

833 **Barkoulas, M., Hay, A., Kougioumoutzi, E. and Tsiantis, M.** (2008). A
834 developmental framework for dissected leaf formation in the Arabidopsis
835 relative Cardamine hirsuta. *Nat Genet* **40**, 1136–1141.

836 **Bayer, E. M., Bayer, E. M., Smith, R. S., Mandel, T., Nakayama, N., Sauer, M.,**
837 **Prusinkiewicz, P. and Kuhlemeier, C.** (2009). Integration of transport-based
838 models for phyllotaxis and midvein formation. *Genes Dev* **23**, 373–384.

839 **Benková, E., Michniewicz, M., Sauer, M., Teichmann, T., Seifertová, D.,**
840 **Jürgens, G. and Friml, J.** (2003). Local, Efflux-Dependent Auxin Gradients
841 as a Common Module for Plant Organ Formation. *Cell* **115**, 591–602.

842 **Bennett, S. R. M., Alvarez, J., Bossinger, G. and Smyth, D. R.** (1995).
843 Morphogenesis in pinoid mutants of Arabidopsis thaliana. *Plant J* **8**, 505–520.

844 **Bennett, T. A., Brockington, S. F., Rothfels, C., Graham, S. W., Stevenson,**
845 **D., Kutchan, T., Rolf, M., Thomas, P., Wong, G. K.-S., Leyser, H. M. O., et**
846 **al.** (2014). Paralogous radiations of PIN proteins with multiple origins of
847 noncanonical PIN structure. *Molecular Biology and Evolution* **31**, 2042–2060.

848 **Bennett, T. A., Hines, G., van Rongen, M., Waldie, T., Sawchuk, M. G.,**
849 **Scarpella, E., Ljung, K. and Leyser, H. M. O.** (2016). Connective Auxin
850 Transport in the Shoot Facilitates Communication between Shoot Apices.
851 *PLoS Biol* **14**, e1002446.

852 **Bennett, T. A., Sieberer, T., Willett, B., Booker, J., Luschnig, C. and Leyser,**
853 **H. M. O.** (2006). The Arabidopsis MAX Pathway Controls Shoot Branching by

854 Regulating Auxin Transport. *Current Biology* **16**, 553–563.

855 **Bhatia, N., Bozorg, B., Larsson, A., Ohno, C., Jönsson, H. and Heisler, M. G.**
856 (2016). Auxin Acts through MONOPTEROS to Regulate Plant Cell Polarity
857 and Pattern Phyllotaxis. *Curr Biol* **26**, 3202–3208.

858 **Bilsborough, G. D., Runions, A., Barkoulas, M., Jenkins, H. W., Hasson, A.,**
859 **Galinha, C., Laufs, P., Hay, A., Prusinkiewicz, P. and Tsiantis, M.** (2011).
860 Model for the regulation of Arabidopsis thaliana leaf margin development.
861 *Proc Natl Acad Sci USA* **108**, 3424–3429.

862 **Blilou, I., Xu, J., Wildwater, M., Willemsen, V., Paponov, I., Friml, J.,**
863 **Heidstra, R., Aida, M., Palme, K. and Scheres, B.** (2005). The PIN auxin
864 efflux facilitator network controls growth and patterning in Arabidopsis roots.
865 *Nature* **433**, 39–44.

866 **Bragg, J. N., Anderton, A., Nieu, R. and Vogel, J. P.** (2015). Brachypodium
867 distachyon. *Methods Mol Biol* **1223**, 17–33.

868 **Brunoud, G., Wells, D. M., Oliva, M., Larrieu, A., Mirabet, V., Burrow, A. H.,**
869 **Beeckman, T., Kepinski, S., Traas, J., Bennett, M. J., et al.** (2012). A novel
870 sensor to map auxin response and distribution at high spatio-temporal
871 resolution. *Nature* **482**, 103–106.

872 **Chen, M.-K., Wilson, R. L., Palme, K., Ditengou, F. A. and Shpak, E. D.**
873 (2013). ERECTA family genes regulate auxin transport in the shoot apical
874 meristem and forming leaf primordia. *Plant Physiol* **162**, 1978–1991.

875 **Crawford, S., Shinohara, N., Sieberer, T., Williamson, L., George, G.,**
876 **Hepworth, J., Muller, D., Domagalska, M. A. and Leyser, H. M. O.** (2010).
877 Strigolactones enhance competition between shoot branches by dampening
878 auxin transport. *Development* **137**, 2905–2913.

879 **Deb, Y., Marti, D., Frenz, M., Kuhlemeier, C. and Reinhardt, D.** (2015).
880 Phyllotaxis involves auxin drainage through leaf primordia. *Development* **142**,
881 dev.121244–2001.

882 **Derbyshire, P. and Byrne, M. E.** (2013). MORE SPIKELETS1 is required for
883 spikelet fate in the inflorescence of Brachypodium. *Plant Physiol* **161**, 1291–
884 1302.

885 **Fu, Y., Sander, J. D., Reyon, D., Cascio, V. M. and Joung, J. K.** (2014).
886 Improving CRISPR-Cas nuclease specificity using truncated guide RNAs. *Nat*
887 *Biotechnol* **32**, 279–284.

888 **Gälweiler, L., Guan, C., Müller, A., Wisman, E., Mendgen, K., Yephremov, A.**
889 **and Palme, K.** (1998). Regulation of Polar Auxin Transport by AtPIN1 in
890 Arabidopsis Vascular Tissue. *Science* **282**, 2226–2230.

891 **Gordon, S. P., Heisler, M. G., Reddy, G. V., Ohno, C., Das, P. and**
892 **Meyerowitz, E. M.** (2007). Pattern formation during de novo assembly of the
893 Arabidopsis shoot meristem. *Development* **134**, 3539–3548.

894 **Guenot, B., Bayer, E. M., Bayer, E., Kierzkowski, D., Smith, R. S., Mandel, T.,**
895 **Zádníková, P., Benková, E. and Kuhlemeier, C.** (2012). Pin1-independent
896 leaf initiation in Arabidopsis. *Plant Physiol* **159**, 1501–1510.

897 **Habets, M. E. J. and Offringa, R.** (2014). PIN-driven polar auxin transport in
898 plant developmental plasticity: a key target for environmental and
899 endogenous signals. *New Phytologist* **203**, 362–377.

900 **Heisler, M. G., Hamant, O., Krupinski, P., Uyttewaal, M., Ohno, C., Jönsson,**
901 **H., Traas, J. and Meyerowitz, E. M.** (2010). Alignment between PIN1 polarity
902 and microtubule orientation in the shoot apical meristem reveals a tight
903 coupling between morphogenesis and auxin transport. *PLoS Biol* **8**,
904 e1000516.

905 **Heisler, M. G., Ohno, C., Das, P., Sieber, P., Reddy, G. V., Long, J. A. and**
906 **Meyerowitz, E. M.** (2005). Patterns of auxin transport and gene expression
907 during primordium development revealed by live imaging of the Arabidopsis
908 inflorescence meristem. *Curr Biol* **15**, 1899–1911.

909 **Jia, W., Li, B., Li, S., Liang, Y., Wu, X., Ma, M., Wang, J., Gao, J., Cai, Y.,**
910 **Zhang, Y., et al.** (2016). Mitogen-Activated Protein Kinase Cascade MKK7-
911 MPK6 Plays Important Roles in Plant Development and Regulates Shoot
912 Branching by Phosphorylating PIN1 in Arabidopsis. *PLoS Biol* **14**, e1002550.

913 **Jönsson, H., Heisler, M. G., Shapiro, B. E., Meyerowitz, E. M. and Mjolsness,**
914 **E.** (2006). An auxin-driven polarized transport model for phyllotaxis. *Proc Natl*
915 *Acad Sci USA* **103**, 1633–1638.

916 **Kierzkowski, D., Lenhard, M., Smith, R. S. and Kuhlemeier, C.** (2013).
917 Interaction between meristem tissue layers controls phyllotaxis. *Dev Cell* **26**,
918 616–628.

919 **Kleine-Vehn, J., Dhonukshe, P., Sauer, M., Brewer, P. B., Wisniewska, J.,**
920 **Paciorek, T., Benková, E. and Friml, J.** (2008a). ARF GEF-dependent
921 transcytosis and polar delivery of PIN auxin carriers in Arabidopsis. *Curr Biol*
922 **18**, 526–531.

923 **Kleine-Vehn, J., Leitner, J., Zwiewka, M., Sauer, M., Abas, L., Luschnig, C.**
924 **and Friml, J.** (2008b). Differential degradation of PIN2 auxin efflux carrier by
925 retromer-dependent vacuolar targeting. *Proc Natl Acad Sci USA* **105**, 17812–
926 17817.

927 **Knöller, A. S., Blakeslee, J. J., Richards, E. L., Peer, W. A. and Murphy, A. S.**
928 (2010). Brachytic2/ZmABCB1 functions in IAA export from intercalary
929 meristems. *J Exp Bot* **61**, 3689–3696.

930 **Lenhard, M. and Laux, T.** (2003). Stem cell homeostasis in the Arabidopsis
931 shoot meristem is regulated by intercellular movement of CLAVATA3 and its
932 sequestration by CLAVATA1. *Development* **130**, 3163–3173.

933 **Leyser, H. M. O.** (2005). Auxin Distribution and Plant Pattern Formation: How
934 Many Angels Can Dance on the Point of PIN? *Cell* **121**, 819–822.

935 **Leyser, H. M. O.** (2006). Dynamic integration of auxin transport and signalling.
936 *CURBIO* **16**, R424–33.

937 **Leyser, H. M. O.** (2010). The power of auxin in plants. *Plant Physiol* **154**, 501–
938 505.

939 **Luschnig, C. and Vert, G.** (2014). The dynamics of plant plasma membrane
940 proteins: PINs and beyond. *Development* **141**, 2924–2938.

941 **Martinez, C. C., Koenig, D., Chitwood, D. H. and Sinha, N. R.** (2016). A sister
942 of PIN1 gene in tomato (Solanum lycopersicum) defines leaf and flower organ
943 initiation patterns by maintaining epidermal auxin flux. *Dev Biol* **419**, 85–98.

944 **Miao, J., Guo, D., Zhang, J., Huang, Q., Qin, G., Zhang, X., Wan, J., Gu, H.**
945 **and Qu, L.-J.** (2013). Targeted mutagenesis in rice using CRISPR-Cas
946 system. *Cell Res* **23**, 1233–1236.

947 **Mitchison, G. J.** (1980). A Model for Vein Formation in Higher Plants. *Proc. Biol.*
948 *Sci.* **207**, 79–109.

949 **Mitchison, G. J., Hanke, D. E. and Sheldrake, A. R.** (1981). The Polar
950 Transport of Auxin and Vein Patterns in Plants [and Discussion].
951 *Philosophical Transactions of the Royal Society B: Biological Sciences* **295**,
952 461–471.

953 **Moore, I., Gälweiler, L., Grosskopf, D. and Palme, K.** (1998). A transcription
954 activation system for regulated gene expression in transgenic plants. *Proc.*
955 *Natl. Acad. Sci. U.S.A.* **95**, 376–381.

956 **Multani, D. S., Briggs, S. P., Chamberlin, M. A., Blakeslee, J. J., Murphy, A.**
957 **S. and Johal, G. S.** (2003). Loss of an MDR transporter in compact stalks of
958 maize br2 and sorghum dw3 mutants. *Science* **302**, 81–84.

959 **O'Connor, D. L., Runions, A., Sluis, A., Bragg, J., Vogel, J. P.,**
960 **Prusinkiewicz, P. and Hake, S.** (2014). A division in PIN-mediated auxin
961 patterning during organ initiation in grasses. *PLoS Comput Biol* **10**,
962 e1003447.

963 **Okada, K., Ueda, J., Komaki, M. K., Bell, C. J. and Shimura, Y.** (1991).
964 Requirement of the Auxin Polar Transport System in Early Stages of
965 Arabidopsis Floral Bud Formation. *The Plant Cell* **3**, 677–684.

966 **Paponov, I. A., Teale, W. D. and Trebar, M.** (2005). The PIN auxin efflux
967 facilitators: evolutionary and functional perspectives. *Trends Plant Sci* **10**,
968 170–177.

969 **Prusinkiewicz, P., Crawford, S., Smith, R. S., Ljung, K., Bennett, T. A.,**
970 **Ongaro, V. and Leyser, H. M. O.** (2009). Control of bud activation by an
971 auxin transport switch. *Proc Natl Acad Sci USA* **106**, 17431–17436.

972 **Raven, J. A.** (1975). Transport of indoleacetic acid in plant cells in relation to pH
973 and electrical potential gradients, and its significance for polar IAA transport.
974 *New Phytol* **74**, 163–172.

975 **Reinhardt, D., Mandel, T. and Kuhlemeier, C.** (2000). Auxin Regulates the
976 Initiation and Radial Position of Plant Lateral Organs. *The Plant Cell* **12**, 507.

977 **Reinhardt, D., Pesce, E.-R., Stieger, P., Mandel, T., Baltensperger, K.,**
978 **Bennett, M. J., Traas, J., Friml, J. and Kuhlemeier, C.** (2003). Regulation of
979 phyllotaxis by polar auxin transport. *Nature* **426**, 255–260.

980 **Rubery, P. H. and Sheldrake, A. R.** (1974). Carrier-mediated auxin transport.
981 *Planta* **118**, 101–121.

982 **Sauer, M., Balla, J., Luschnig, C., Wisniewska, J., Reinöhl, V., Friml, J. and**
983 **Benková, E.** (2006). Canalization of auxin flow by Aux/IAA-ARF-dependent
984 feedback regulation of PIN polarity. *Genes Dev* **20**, 2902–2911.

985 **Sawchuk, M. G., Edgar, A. and Scarpella, E.** (2013). Patterning of Leaf Vein
986 Networks by Convergent Auxin Transport Pathways. *PLoS Genet* **9**,
987 e1003294.

988 **Scarpella, E., Marcos, D., Friml, J. and Berleth, T.** (2006). Control of leaf
989 vascular patterning by polar auxin transport. *Genes Dev* **20**, 1015–1027.

990 **Sessions, A., Weigel, D. and Yanofsky, M. F.** (2002). The Arabidopsis thaliana
991 MERISTEM LAYER 1 promoter specifies epidermal expression in meristems
992 and young primordia. *Plant J* **20**, 259–263.

993 **Shinohara, N., Taylor, C. and Leyser, H. M. O.** (2013). Strigolactone Can
994 Promote or Inhibit Shoot Branching by Triggering Rapid Depletion of the
995 Auxin Efflux Protein PIN1 from the Plasma Membrane. *PLoS Biol* **11**,
996 e1001474.

997 **Smith, R. S., Guyomarc'h, S., Mandel, T., Reinhardt, D., Kuhlemeier, C. and**
998 **Prusinkiewicz, P.** (2006). A plausible model of phyllotaxis. *Proc. Natl. Acad.*
999 *Sci. U.S.A.* **103**, 1301–1306.

1000 **Stoma, S., Lucas, M., Chopard, J., Schaedel, M. and Godin, C.** (2008). Flux-
1001 Based Transport Enhancement as a Plausible Unifying Mechanism for Auxin
1002 Transport in Meristem Development. *PLoS Comput Biol* **4**, e1000207.

1003 **Torii, K. U., Mitsukawa, N., Oosumi, T., Matsuura, Y., Yokoyama, R.,**
1004 **Whittier, R. F. and Komeda, Y.** (1996). The Arabidopsis ERECTA gene
1005 encodes a putative receptor protein kinase with extracellular leucine-rich
1006 repeats. *The Plant Cell* **8**, 735–746.

1007 **Verna, C., Sawchuk, M. G., Linh, N. M. and Scarpella, E.** (2015). Control of
1008 vein network topology by auxin transport. *BMC Biol* **13**, 94.

1009 **Vieten, A., Vanneste, S., Wisniewska, J., Benkova, E., Benjamins, R.,**
1010 **Beeckman, T., Luschnig, C. and Friml, J.** (2005). Functional redundancy of
1011 PIN proteins is accompanied by auxin-dependent cross-regulation of PIN
1012 expression. *Development* **132**, 4521–4531.

1013 **Wang, R. and Estelle, M.** (2014). Diversity and specificity: auxin perception and
1014 signaling through the TIR1/AFB pathway. *Curr Opin Plant Biol* **21**, 51–58.

1015 **Weller, B., Zourelidou, M., Frank, L., Barbosa, I. C. R., Fastner, A., Richter,**
1016 **S., Jürgens, G., Hammes, U. Z. and Schwechheimer, C.** (2017). Dynamic
1017 PIN-FORMED auxin efflux carrier phosphorylation at the plasma membrane
1018 controls auxin efflux-dependent growth. *Proc Natl Acad Sci USA* **114**, E887–
1019 E896.

1020 **Willige, B. C., Ahlers, S., Zourelidou, M., Barbosa, I. C. R., Demarsy, E.,**
1021 **Trevisan, M., Davis, P. A., Roelfsema, M. R. G., Hangarter, R.,**
1022 **Fankhauser, C., et al.** (2013). D6PK AGCVIII kinases are required for auxin
1023 transport and phototropic hypocotyl bending in Arabidopsis. *The Plant Cell*
1024 **25**, 1674–1688.

1025 **Wisniewska, J., Xu, J., Seifertová, D., Brewer, P. B., Ruzicka, K., Blilou, I.,**
1026 **Rouquié, D., Benková, E., Scheres, B. and Friml, J.** (2006). Polar PIN
1027 localization directs auxin flow in plants. *Science* **312**, 883–883.

1028 **Xu, J., Hofhuis, H., Heidstra, R., Sauer, M., Friml, J. and Scheres, B.** (2006).
1029 A molecular framework for plant regeneration. *Science* **311**, 385–388.

1030 **Zhou, C., Han, L., Hou, C., Metelli, A., Qi, L., Tadege, M., Mysore, K. S. and**
1031 **Wang, Z.-Y.** (2011). Developmental analysis of a Medicago truncatula
1032 smooth leaf margin1 mutant reveals context-dependent effects on compound
1033 leaf development. *The Plant Cell* **23**, 2106–2124.

1034

1035

1036 # Figures and Legends

1037 **Figure 1. Mutation of SoPIN1 but not PIN1a and PIN1b severely effects organ**
1038 **initiation in Brachypodium. (A)** *SoPIN1*, *PIN1a*, and *PIN1b* CRISPR-derived mutant
1039 alleles (see methods). Coding sequences are indicated by grey boxes. Arrowheads
1040 indicate CRISPR target sites and are labeled with the type of DNA lesion (C insertion, T
1041 insertion, or A deletion). All mutant alleles have frame shifts that result in premature
1042 stop codons at the positions indicated. **(B-G)** Inflorescence phenotypes of CRISPR-
1043 derived *sopin1-1, pin1a-1*, and *pin1b-1* mutants. See Figure 2 for whole-plant
1044 phenotypes. **(B-E)** and **(G)** are scanning electron microscopy (SEM). **(B)** Immature wild-
1045 type (WT) (inbred line Bd21-3) Brachypodium inflorescence with several lateral spikelet
1046 meristems (lsm), and a terminal spikelet meristem (tsm). **(C)** *sopin1-1* plants have
1047 severe organ initiation defects in the inflorescence. **(D)** Detail of a wild-type lateral
1048 spikelet meristem outlined by a box in **(B)** showing an immature lemma (l), which is the
1049 leaf-like organ that subtends the floral meristem (fm). **(E)** Detail of barren lateral spikelet
1050 meristem outlined by box in **(C). (F)** Mature inflorescence phenotypes of WT (Inbred
1051 Bd21-3), *sopin1-1, pin1a-1, pin1b-1,* and double *pin1a-1 / pin1b-1* mutants. The terminal
1052 spikelet (ts) of each inflorescence is indicated for comparison. Arrowhead indicates bent
1053 internode tissue in *pin1b-1.* Genotypes for **(G-I)** are indicated at the bottom of **(I). (G)**
1054 SEM details of representative spikelet meristems**. (H)** Box-plot of total whole-plant
1055 spikelet number at seed-set. (n = 22-53 plants each genotype). Samples with different
1056 letters are significantly different from each other (ANOVA, Tukey HSD, $p < 0.05$). See
1057 "Figure 1 H-I Source Data 1" for source data. **(I)** Box-plot of the number of florets in
1058 each terminal spikelet of the central branch at seed set. (n = 22-53 plants each

1059 genotype). Samples with different letters are significantly different from each other
1060 (ANOVA, Tukey HSD, $p < 0.05$). See “Figure 1 H-I Source Data 1” for source data. **(J)**
1061 Medial confocal Z-section of pZmUbi::DII-Venus (DII) expression in a WT spikelet co-
1062 expressing SoPIN1 tagged with Cerulean (a CFP variant) under the native *SoPIN1*
1063 promoter. Organ primordia are numbered I2, I1, P1 from youngest to oldest. DII is
1064 normally degraded at SoPIN1 convergence points in I2 and I1 primordia (asterisks), and
1065 in response to auxin treatment (See Figure 1 – supplement 2). Inset shows color look-
1066 up-table for all subsequent PIN images and color look-up-table for DII. **(K)** Medial
1067 confocal Z-section of pZmUbi::DII-Venus expression in a *sopin1-1* spikelet meristem.
1068 DII degradation does not occur in the periphery of *sopin1-1* meristems, and organs fail
1069 to initiate (arrow). Scale bars: 100μm in **(B)** and **(C)**, 20μm in **(D)** and **(E),** 1cm in **(F),**
1070 50μm each in **(G),** and 25μm in **(J)** and **(K).**
1071
1072 **Figure 1 – supplement 1. *sopin1-1* is complemented by the SoPIN1-CIT reporter.**
1073 **(A)** Wild-type inflorescence (Bd21-3 background) with wild-type mature spikelets (s). **(B)**
1074 *sopin1-1* inflorescence with an aborted spikelet (asterisk) and several barren white
1075 spikelet nodes (n). Green internode (i) tissue is also labeled. **(C)** Inflorescence of a
1076 *sopin1-1* mutant plant complemented by previously published full-length SoPIN1
1077 internal CITRINE fluorescent protein fusion under the native *SoPIN1* promoter
1078 (+SoPIN1-CIT) (O'Connor et al., 2014). Scale bars: 1cm.
1079
1080 **Figure 1 – supplement 2. DII-Venus is degraded in the presence of auxin in**
1081 **Brachypodium spikelet meristems. (A)** 1 μM NAA-treated, and **(B)** mock-treated

1082 spikelet meristems expressing pZmUbi::DII-Venus imaged every 30 min after treatment.
1083 Images from left to right, pre-treatment expression, 30 min, 60 min and 90 min time-
1084 points. **(C)** Relative mean fluorescence in a radius at the spikelet meristem tip in NAA-
1085 treated and Mock samples at 0, 30, 60 and 90-minute time points. Scale bars: 25µm.
1086
1087 **Figure 1 - Source Data 1.** Source data for spikelet and floret counts in Figure 1 H-I.
1088
1089 **Figure 1 – Source Data 2.** Source data for DII quantification in Figure 1 – supplement 2
1090 panel C.
1091
1092

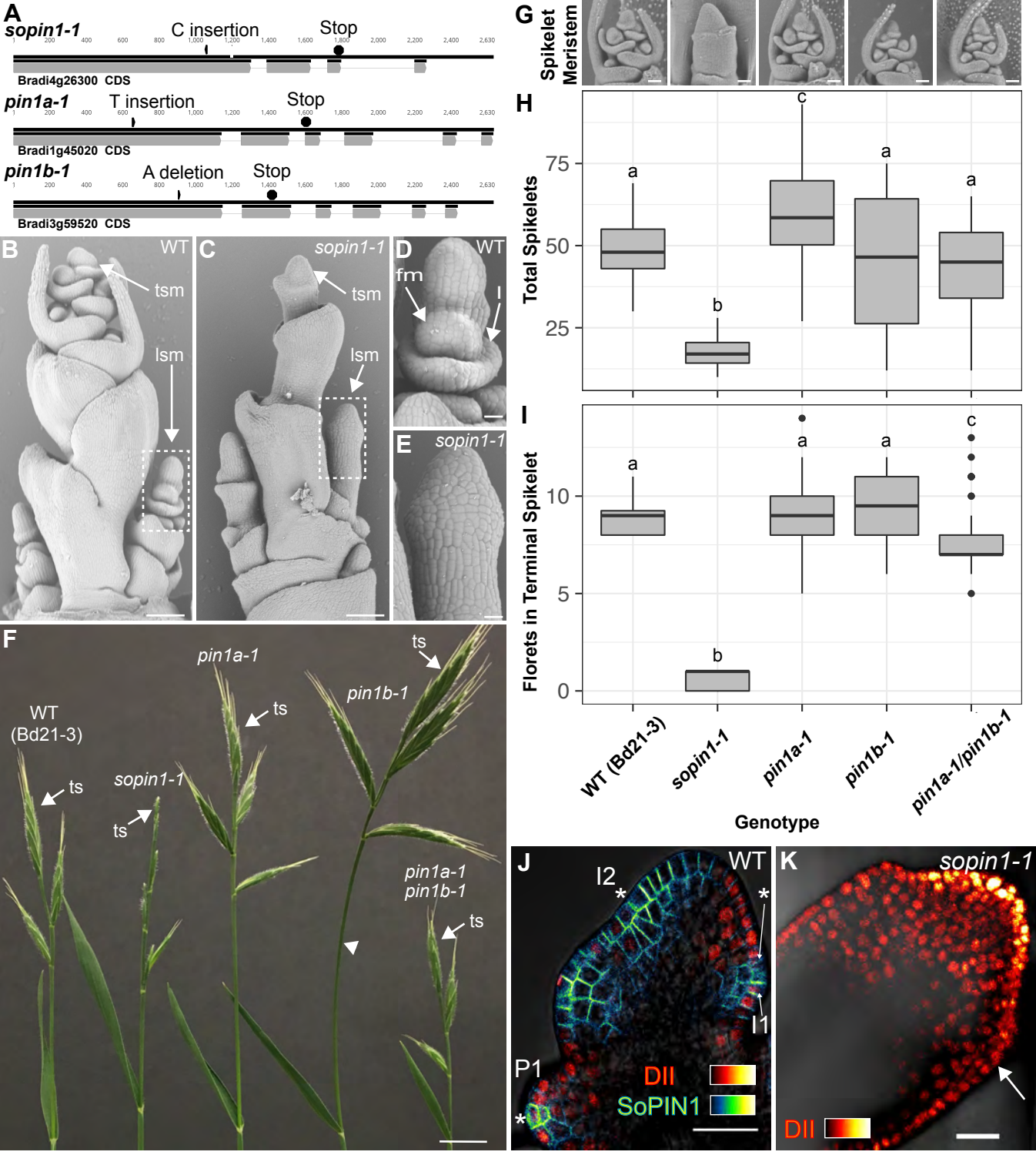
A
sopin1-1
C insertion
Stop
Bradi4g26300 CDS
pin1a-1
T insertion
Stop
Bradi1g45020 CDS
pin1b-1
A deletion
Stop
Bradi3g59520 CDS
B
WT
tsm
lsm
C
sopin1-1
tsm
lsm
D
WT
fm
l
E
sopin1-1
F
WT
(Bd21-3)
ts
sopin1-1
ts
pin1a-1
ts
pin1b-1
ts
pin1a-1
pin1b-1
ts
G
Spikelet
Meristem
H
Total Spikelets
75
50
25
a
b
c
a
a
I
Florets in Terminal Spikelet
10
5
0
a
b
a
a
c
WT (Bd21-3)
sopin1-1
pin1a-1
pin1b-1
pin1a-1/pin1b-1
Genotype
J
WT
I2
I1
P1
DII
SoPIN1
K
sopin1-1
DII

**Figure 1**

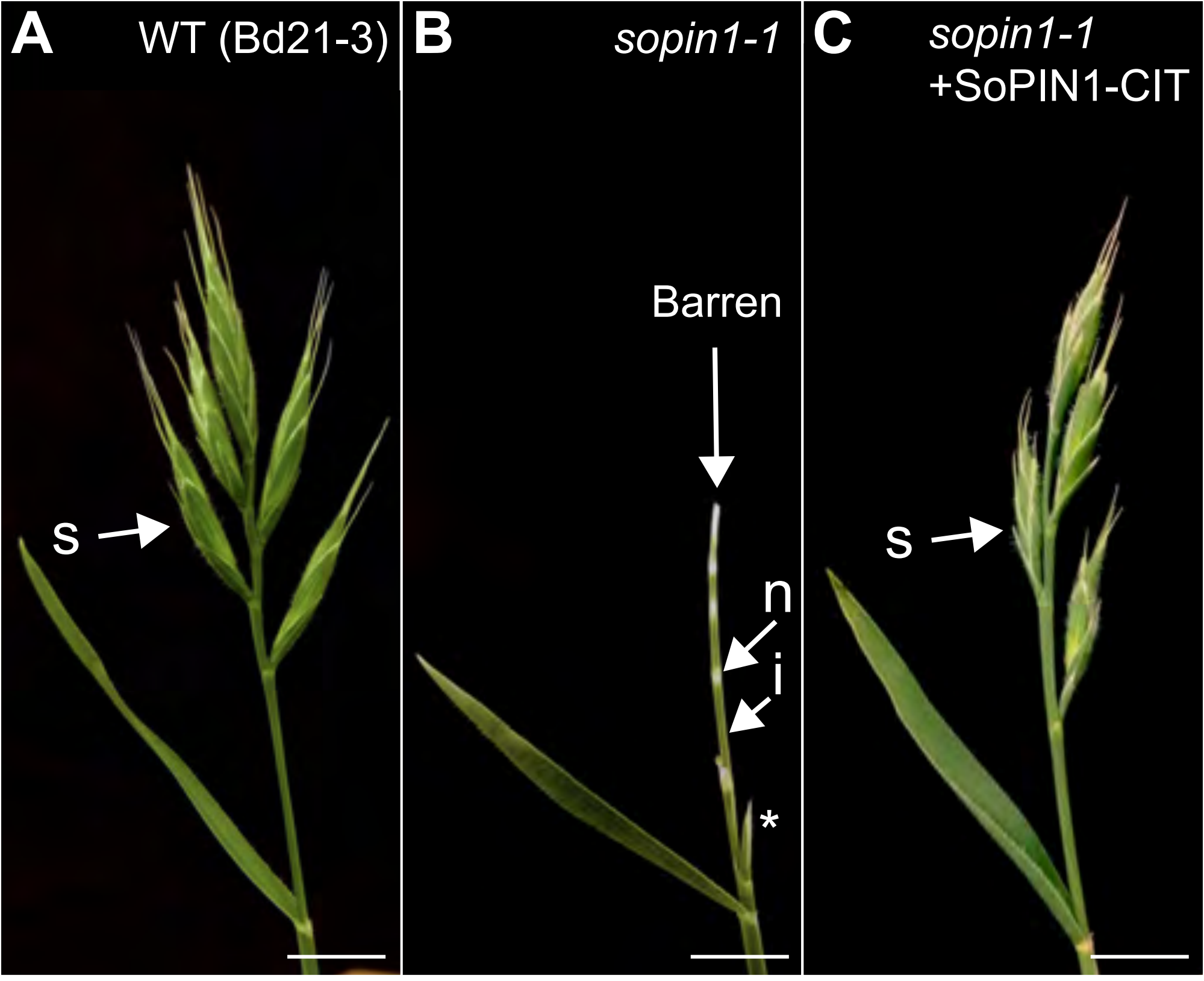


**Figure 1 - supplement 1**

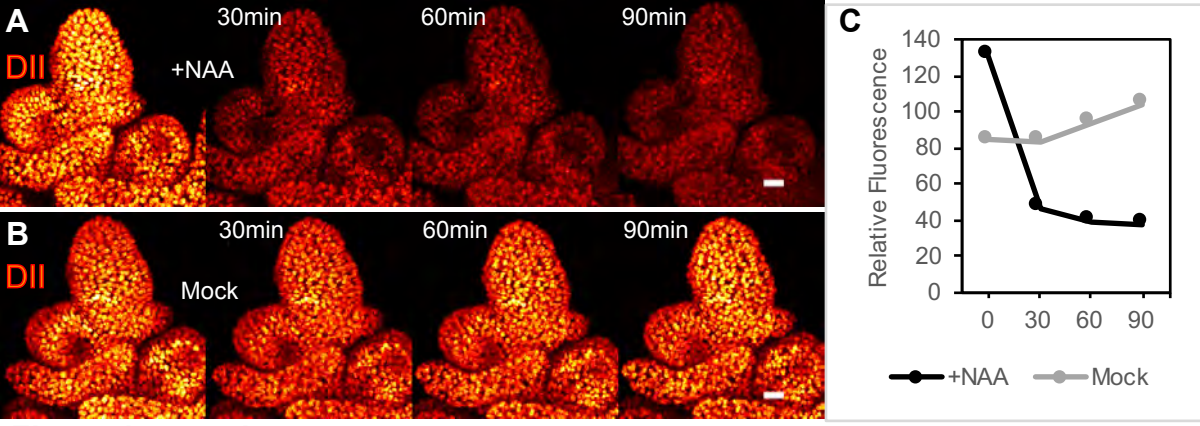


**Figure 1 - supplement 2**

1093 **Figure 2 - PIN1a and PIN1b redundantly control internode growth in**
1094 **Brachypodium. (A-D)** Whole-plant phenotypes for WT (Bd21-3), *pin1a-1*, *pin1b-1*, and
1095 double *pin1a-1 / pin1b-1* mutants. **(E)** Stacked bar graph of the length of the first 5
1096 internodes below the inflorescence of the main branch, labeled I1-I5 from top to bottom.
1097 Lines connect analogous internodes between genotypes. Analogous internodes with
1098 different letters are significantly different from each other (ANOVA, Tukey HSD, $p <$
1099 $0.05$). I5 internodes were not significantly different between genotypes and are
1100 unlabeled. Internode lengths significantly different from WT are indicated by asterisks.
1101 (n = 18-51 individuals each genotype) See "Figure 2 Source Data 1" for source data.
1102 Scale bars: 1cm in **(A-D)**.
1103
1104 **Figure 2 – supplement 1. PIN1b-CIT-mediated complementation of *pin1b-1***
1105 **internode length defects.** Stacked bar graph of the length of the first 5 internodes
1106 below the inflorescence of the main branch, labeled I1-I5 from top to bottom, for *pin1b-1*
1107 and *pin1b-1* containing the previously published full-length PIN1b internal CITRINE
1108 fluorescent protein fusion under the native *PIN1b* promoter (+PIN1b-CIT) (O'Connor et
1109 al., 2014) (n = 10 each genotype). Lines connect analogous internodes between
1110 genotypes. Internodes that are significantly different between genotypes are marked
1111 with asterisks. The I4 and I5 internodes are significantly shorter in the complemented
1112 line than in *pin1b-1* (ANOVA, Tukey HSD, $p < 0.05$). See "Figure 2 Source Data 2" for
1113 source data.
1114
1115 **Figure 2 Source Data 1.** Source data for internode length measurements in Figure 2E.

1116

1117 **Figure 2 Source Data 2.** Source data for PIN1b-CIT-mediated complementation of

1118 *pin1b-1* internode lengths in Figure 2 - supplement 1.

1119

1120

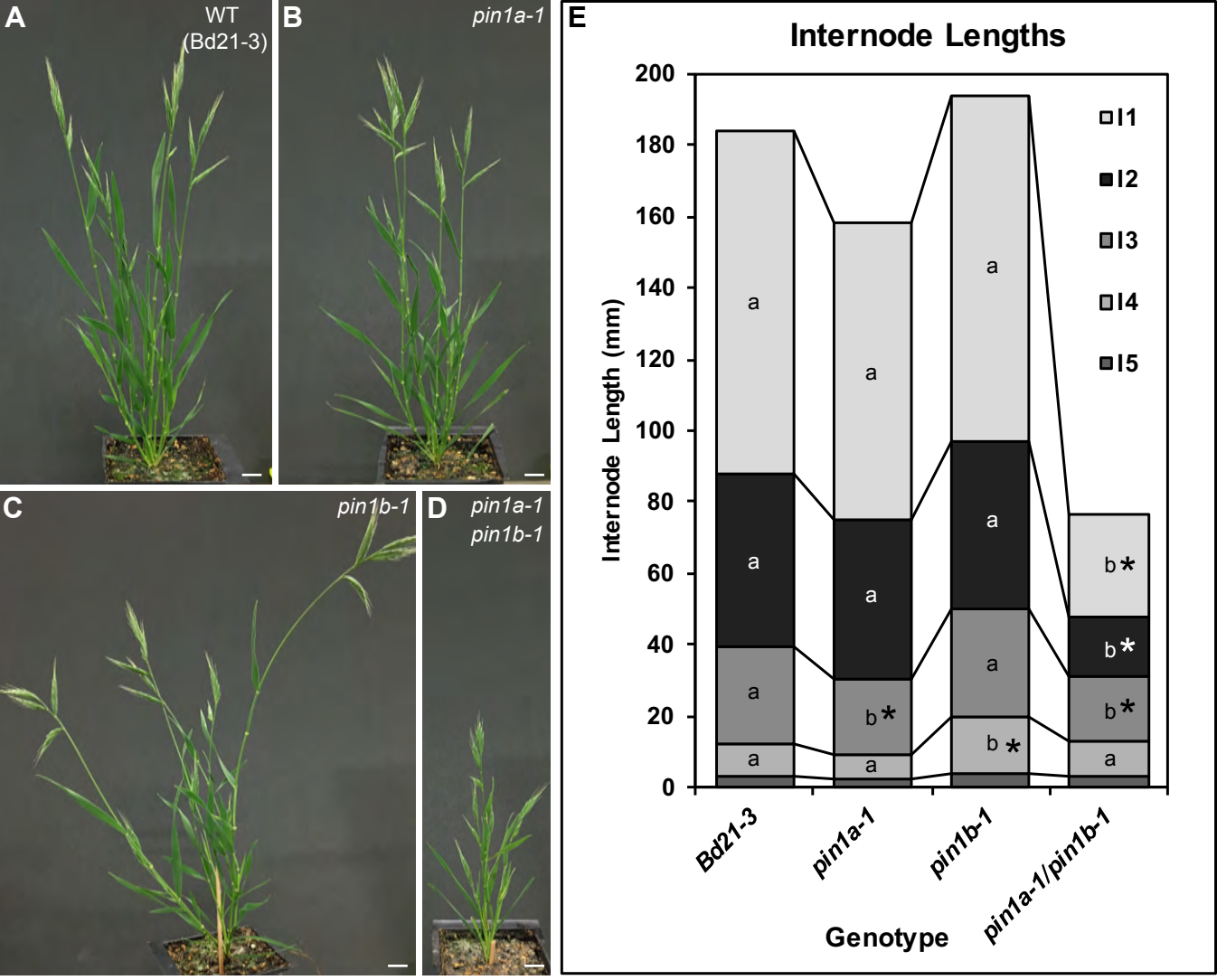
A
WT
(Bd21-3)
B
pin1a-1
C
pin1b-1
D
pin1a-1
pin1b-1
E
Internode Lengths
Internode Length (mm)
200
180
160
140
120
100
80
60
40
20
0
I1
I2
I3
I4
I5
a
b*
Bd21-3
pin1a-1
pin1b-1
pin1a-1/pin1b-1
Genotype

**Figure 2**

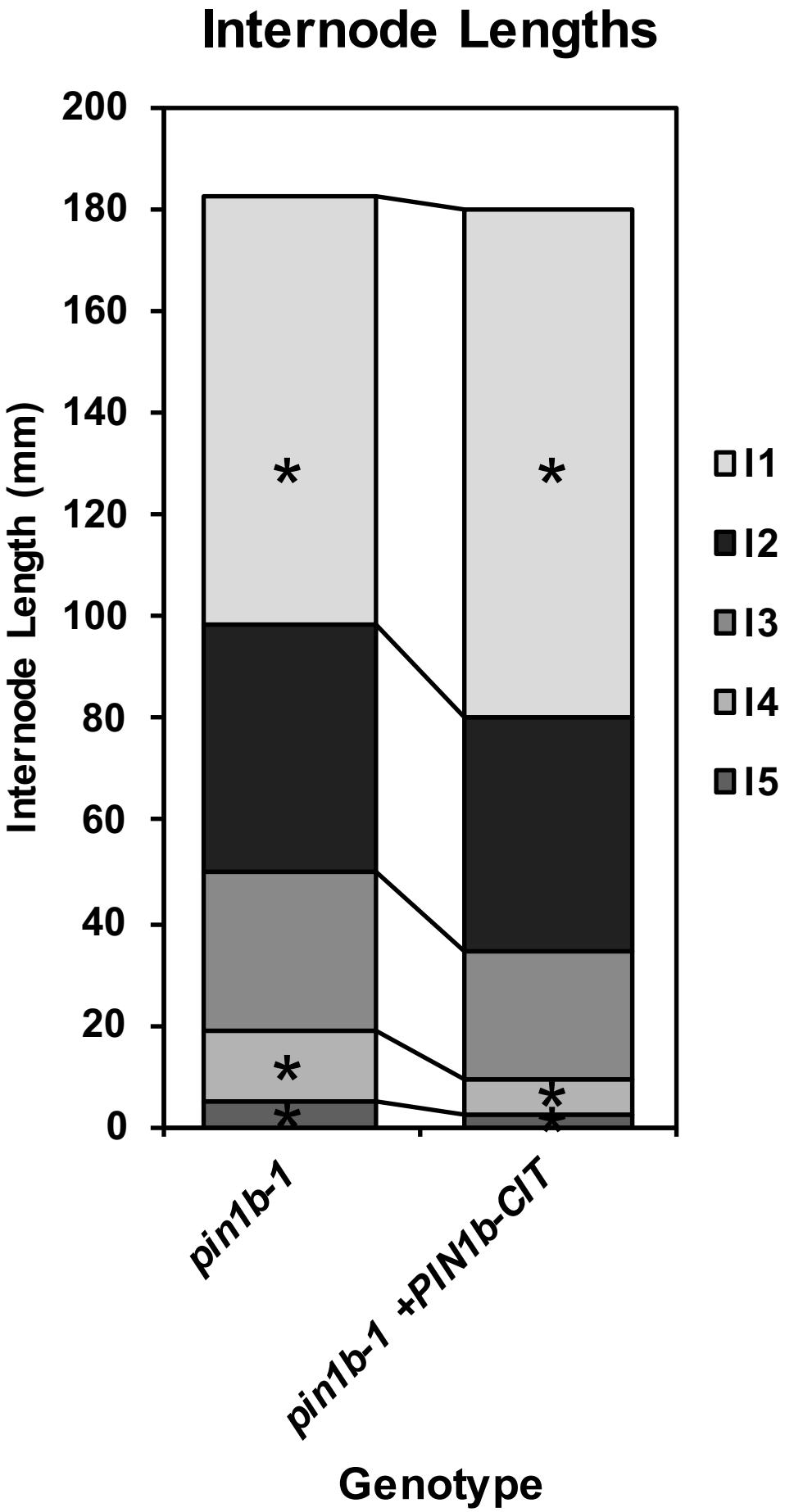


**Figure 2 - supplement 1**

1121 **Figure 3. AtPIN1, SoPIN1, and PIN1b show different behaviors when expressed in**
1122 **wild-type Arabidopsis.** Arabidopsis *AtPIN1* promoter (*proAtPIN1*) driven expression of
1123 GFP-tagged AtPIN1 and CITRINE-tagged (a YFP derivative) SoPIN1 and PIN1b in wild-
1124 type Columbia (Col-0) Arabidopsis. **(A,D,G,J)** AtPIN1, **(B,E,H,K)** SoPIN1, **(C,F,I,L)**
1125 PIN1b. **(A-C)** Maximum projections of meristem apexes. Arrows in (**A)** and **(B)** indicate
1126 convergence points (cp) in I2 primordium. Arrowhead in **(C)** indicates internalized PIN1b
1127 in punctate membrane bodies. The I2 and I1 primordia are labeled. **(D-F)** Tiled confocal
1128 maximum projections of longitudinal hand-sections through inflorescence apexes.
1129 Arrows indicate SoPIN1 epidermal expression in sepal primordia and flower pedicels in
1130 **(E)** and the lack of AtPIN1 and PIN1b epidermal expression in the same tissues in **(D)**
1131 and **(F)**. Box in **(D)** shows detail area in Figure 3 – supplement 1 panel D**. (G-I)** Tiled
1132 confocal maximum projections of longitudinal hand-sections through basal inflorescence
1133 stem internodes 1cm above the rosette. **(J-L)** Tiled confocal maximum projections of
1134 hand cross-sections through basal internodes 1cm above the rosette. Signal at the edge
1135 of each section (arrowheads) is cuticle auto-florescence. The cortex (co), cambium (ca),
1136 xylem parenchyma (xp), and pith (p) tissues are indicated in **(G-L)**. Arrows in **(H)** and
1137 **(K)** indicate cortex and pith ectopic expression of SoPIN1. Red signal in all panels is
1138 chlorophyll auto-florescence. Scale bars: 25μm in **(A-C)**, and 100μm in **(D-L)**.
1139

1140 **Figure 3 – supplement 1. *proAtPIN1* AtPIN1, SoPIN1, and PIN1b expression**
1141 **details. (A)** Confocal z-section of AtPIN1 accumulation in vascular-associated domains
1142 just below the apex of the meristem shown in Figure 3A. **(B)** Confocal z-section of
1143 SoPIN1 accumulation in a ring-shaped domain just below the apex of the meristem

1144 shown in Figure 3B. **(C)** Confocal z-section of PIN1b accumulation in vascular-
1145 associated domains just below the apex of the meristem shown in Figure 3C. (**D)**
1146 Maximum projection detail of AtPIN1 accumulation in both pith (p) and procambium (pc)
1147 tissues in the immature inflorescence stem outlined with a box in Figure 3D. **(E)**
1148 Maximum projection detail of rootward polarized SoPIN1 (arrows) in a longitudinal hand-
1149 section of the basal internode pith tissue. **(F)** Maximum projection detail of rootward
1150 polarized PIN1b (arrows) in a longitudinal hand-section of the basal internode xylem
1151 parenchyma tissue. Red signal in **(D-F)** is chlorophyll auto-florescence. Scale bars:
1152 25µm.
1153
1154

Wildtype (Col-0)

*proAtPIN1*::AtPIN1 | *proAtPIN1*::SoPIN1 | *proAtPIN1*::PIN1b

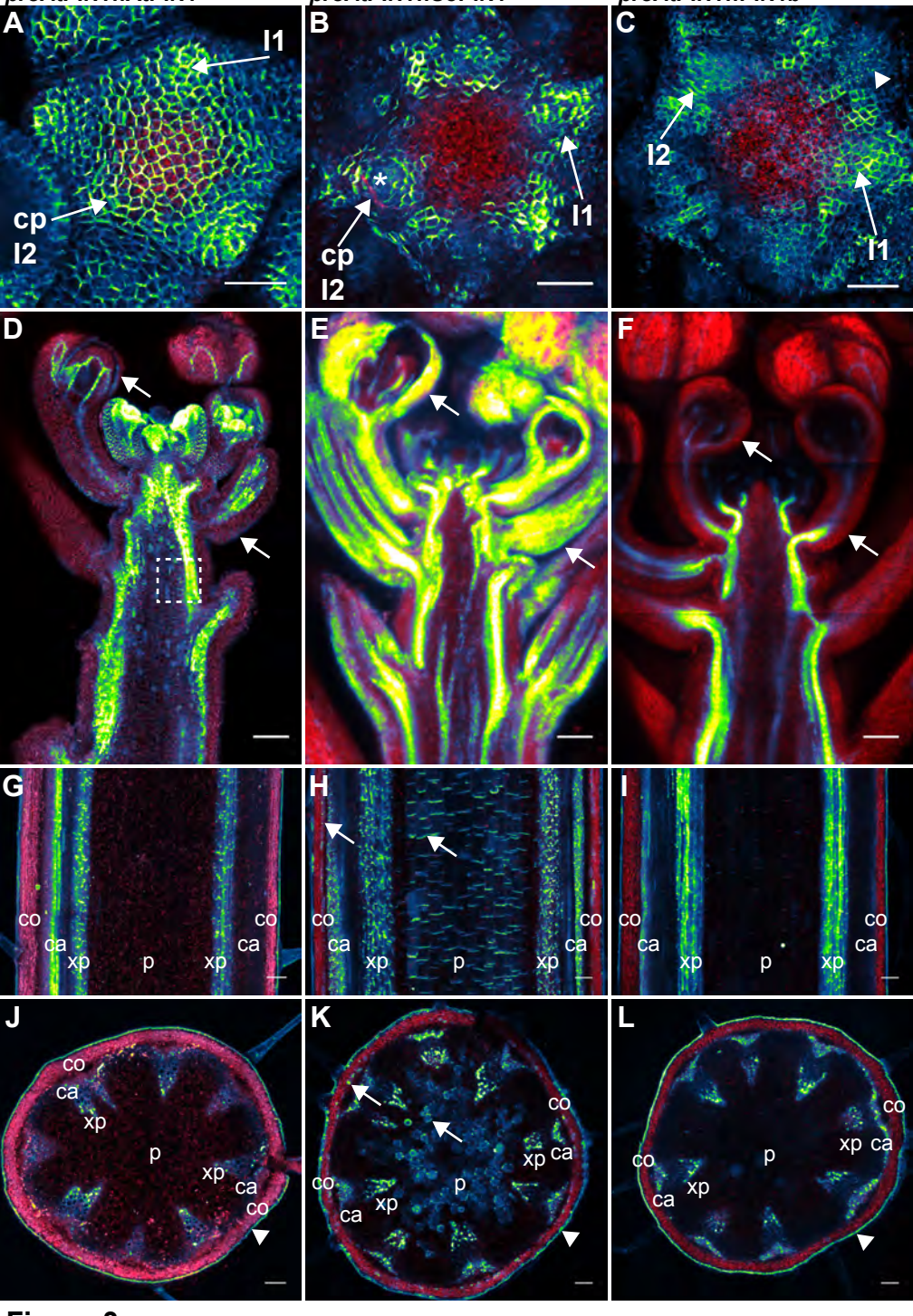


**Figure 3**

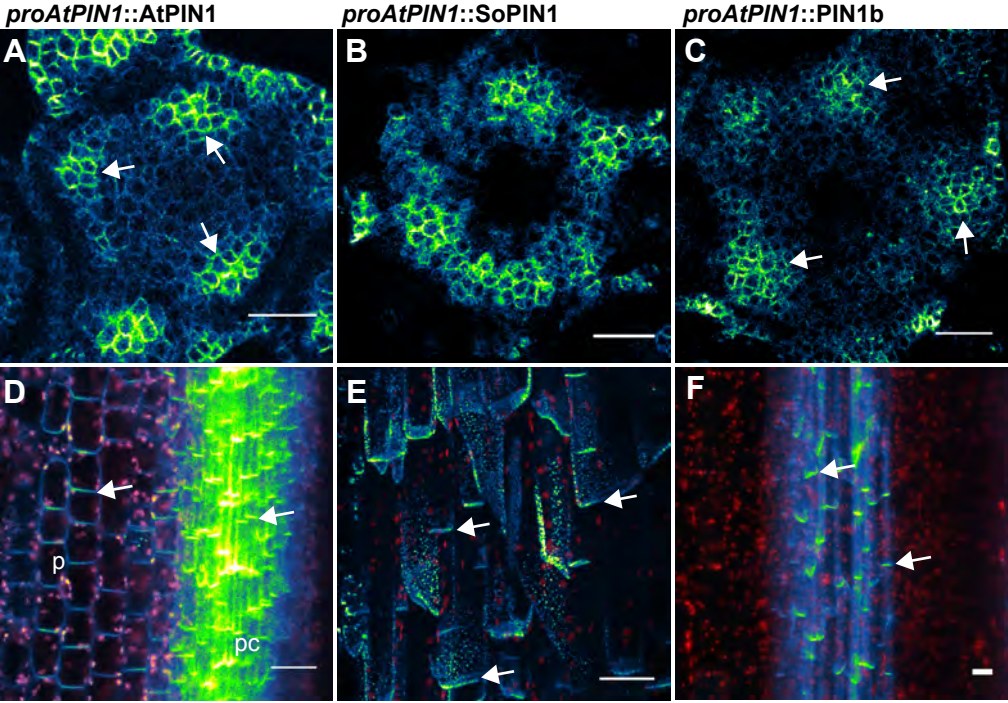


**Figure 3 - supplement 1**

1155 **Figure 4. SoPIN1 but not PIN1b can partially complement the Arabidopsis *pin1-***
1156 ***613* mutant organ initiation and bulk transport defects. (A)** From left to right,
1157 inflorescence phenotypes of WT (Col-0), *proAtPIN1::*SoPIN1 in *pin1-613,*
1158 *proAtPIN1*::PIN1b in *pin1-613,* and *pin1-613* alone. Note that PIN1b-expressing *pin1-*
1159 *613* plants are indistinguishable from *pin1-613* alone. See Figure 4 - supplement 1 for
1160 whole-plant phenotypes. **(B)** Flower (left), and inflorescence apex (right) of WT (Col-0).
1161 **(C)** Flower (left), and inflorescence apex (right) of *proAtPIN1::*SoPIN1 complemented
1162 *pin1-613* mutants. Note the increase in petal number and lack of stamens in the flower,
1163 see Figure 4 - supplement 2 for organ counts. **(D)** Box-plot of bulk auxin transport
1164 (counts per minute, CPM) through basal internodes 1cm above the rosette of 40-day-old
1165 Arabidopsis inflorescence stems. (n=16 each genotype). Samples with different letters
1166 are significantly different from each other (ANOVA, Tukey HSD, $p < 0.05$). See Figure 3
1167 - Source Data 1 for source data. Scale bars: 1cm in **(A)**, 1mm in **(B-C)**.
1168
1169 **Figure 4 - supplement 1. Whole-plant phenotypes of *proAtPIN1*-driven**
1170 **complementation of *pin1-613.*** From left to right, Col-0 (WT), *proAtPIN1::*SoPIN1
1171 complemented *pin1-613*, *proAtPIN1::*PIN1b expressing *pin1-613,* and *pin1-613* alone.
1172 Scale bar: 1cm.
1173
1174 **Figure 4 - supplement 2. Floral organ number in *proAtPIN1::*SoPIN1**
1175 **complemented flowers.** Mean and standard-error of sepal, petal, stamen and carpel
1176 organ numbers in heterozygous *pin1-613* or wild-type (white bars), and

1177 *proAtPIN1::*SoPIN1-complemented *pin1-613* flowers (grey bars) (n=30). See Figure 4 -
1178 Source Data 2 for source data.
1179
1180 **Figure 4 - Source Data 1. Source data for Figure 4D auxin transport assays.**
1181
1182 **Figure 4 - Source Data 2. Source data for Figure 4 - supplement 2 floral organ**
1183 **numbers.**
1184
1185

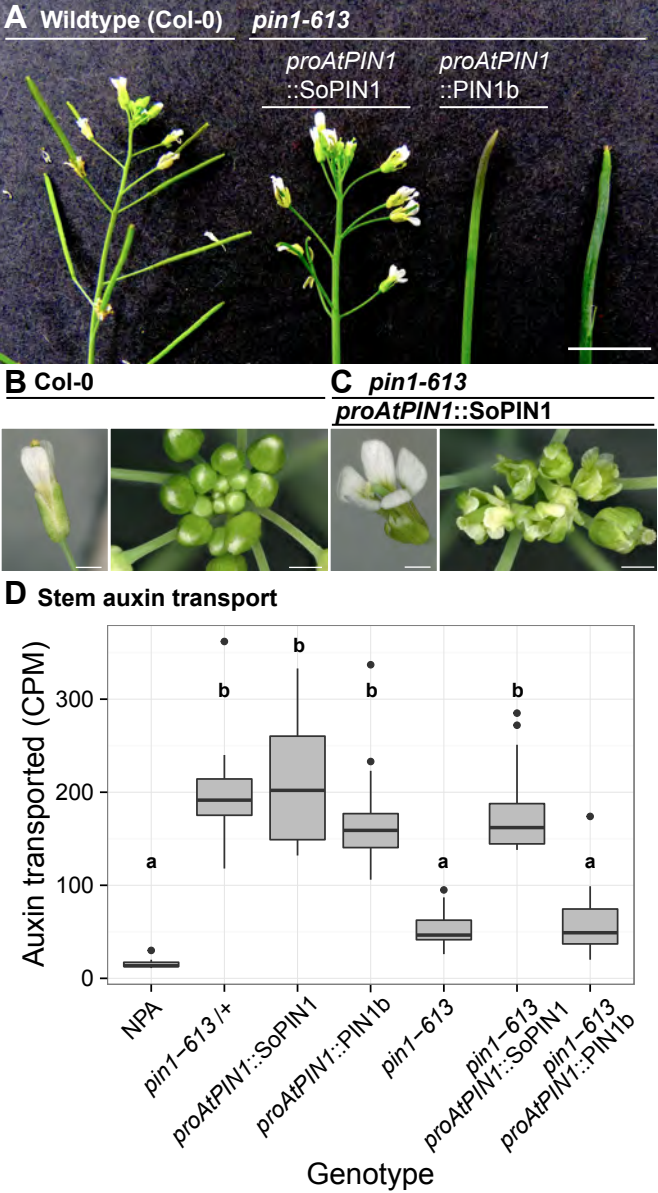
A Wildtype (Col-0)
pin1-613
proAtPIN1 ::SoPIN1
proAtPIN1 ::PIN1b
B Col-0
C pin1-613
proAtPIN1::SoPIN1
D Stem auxin transport
Auxin transported (CPM)
0
100
200
300
a
b
b
b
a
b
a
NPA
pin1−613/+
proAtPIN1::SoPIN1
proAtPIN1::PIN1b
pin1−613
pin1−613 proAtPIN1::SoPIN1
pin1−613 proAtPIN1::PIN1b
Genotype

**Figure 4**

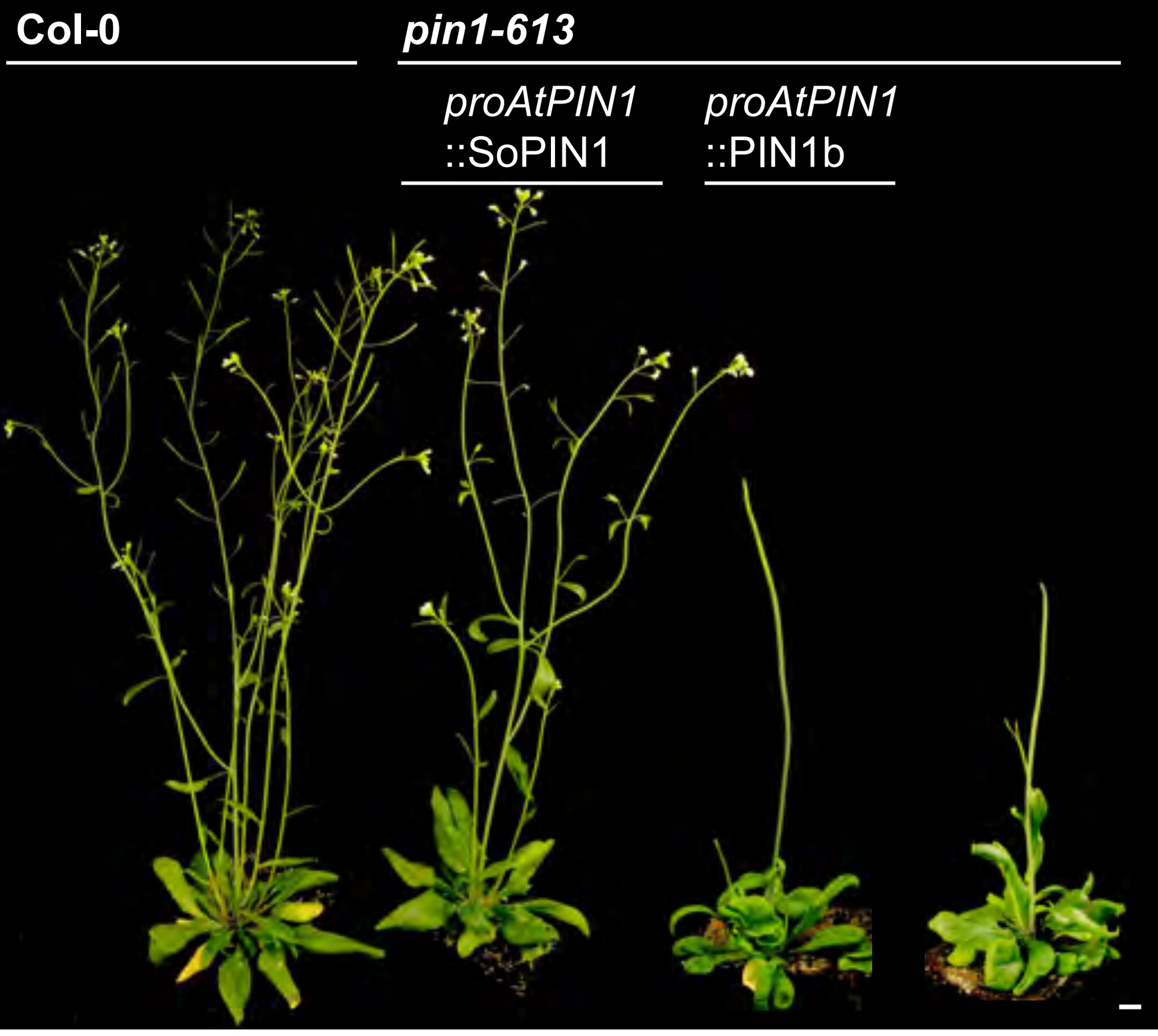


**Figure 4 - supplement 1**

**Floral organ number - *proAtPIN1::*SoPIN1**

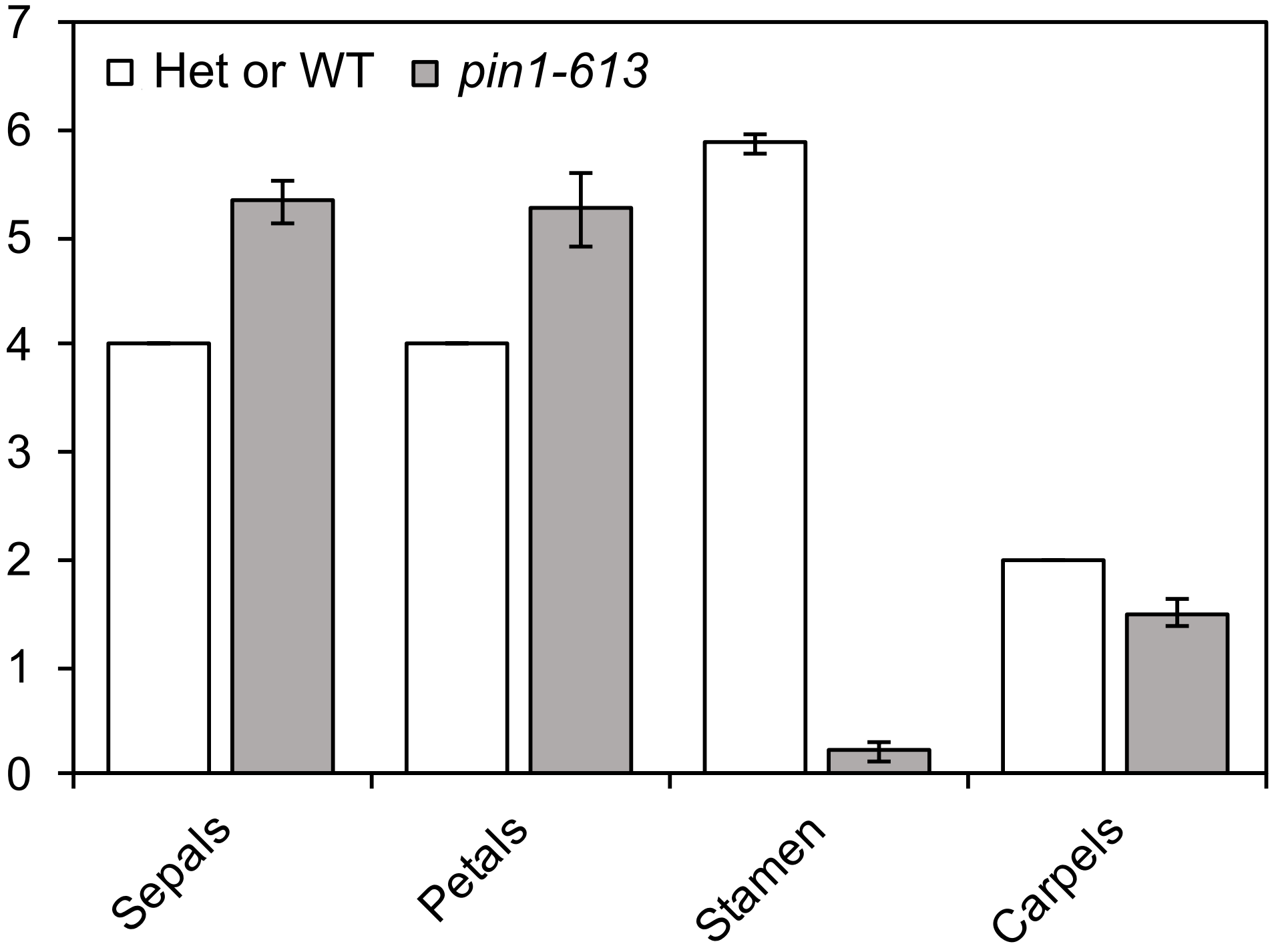


# Figure 4 - supplement 2

1186 **Figure 5. SoPIN1 and PIN1b localization in null *pin1-613* mutants.** Arabidopsis *PIN1*
1187 promoter (*proAtPIN1*) driven expression of Citrine-tagged (YFP derivative) SoPIN1 and
1188 PIN1b in null *pin1-613* mutant tissue. **(A,C,E,G,I)** SoPIN1, **(B,D,F,H,J,K,L,M)** PIN1b. **(A-**
1189 **B)** Maximum projections of meristem apexes. Arrow in **(B)** indicates PIN1b ring shaped
1190 epidermal domain. See Figure 5 – supplement 1 for SoPIN1 expression in a *pin1-613*
1191 segregating family. See Figure 5 – supplement 2 for more examples of PIN1b
1192 expression in *pin1-613* apexes, and Figure 5 – supplement 3 for PIN1b dynamics in
1193 response to auxin addition. **(C-D)** Tiled confocal maximum projections of longitudinal
1194 hand-sections through apexes. Arrow in **(D)** indicates increased PIN1b in the epidermis
1195 in the *pin1-613* background. **(E-F)** Tiled maximum projections of longitudinal hand-
1196 sections through basal inflorescence stem internodes 1cm above the rosette. **(G-H)**
1197 Tiled maximum projections of hand cross-sections through basal internodes 1cm above
1198 the rosette. Signal at the edge of each section (arrowheads) is cuticle auto-florescence.
1199 The cortex (co), cambium (ca), xylem parenchyma (xp), and pith (p) tissues are
1200 indicated in **(E-H).** Arrows in **(E)** and **(G)** indicate cortex and pith accumulation of
1201 SoPIN1. **(I)** Confocal z-section of SoPIN1 accumulation in a ring-shaped domain just
1202 below the apex of a complemented *pin1-613* meristem. **(J)** Longitudinal hand-section of
1203 PIN1b just below a *pin1-613* meristem apex. Arrow shows rootward polarized PIN1b.
1204 **(K)** Detail of polarized PIN1b in the meristem epidermis of a *pin1-613* meristem apex.
1205 **(L)** Cross-section of PIN1b (arrow) in distinct bundles 2mm below a *pin1-613* meristem
1206 apex. **(M)** Rootward polarization of PIN1b (arrow) 3-4 mm below the apex of a *pin1-613*
1207 meristem. Red signal in all panels is chlorophyll auto-florescence. Scale bars: 25μm in
1208 **(A-B),** 100μm in **(C-H),** and 25μm in **(I-M)**.

1209

1210 **Figure 5 – supplement 1. *proAtPIN1::*SoPIN1 expression in *pin1-613* segregating**
1211 **family. (A)** *proAtPIN1::*SoPIN1 expression in 6 different WT or heterozygous *pin1-613*
1212 meristem samples. **(B)** *proAtPIN1::*SoPIN1 expression in 6 different complemented
1213 *pin1-613* meristems. All samples were imaged with identical settings to show the
1214 increase in SoPIN1 accumulation in the *pin1-613* mutant background. Red signal is
1215 chlorophyll auto-florescence. Scale bars: 25µm.

1216

1217 **Figure 5 – supplement 2. *proAtPIN1::*PIN1b expression in *pin1-613* apexes.** Two
1218 representative meristems each from four different transgenic events. All samples were
1219 imaged with identical settings. Scale bars: 25µm.

1220

1221 **Figure 5 – supplement 3. *proAtPIN1::*PIN1b dynamics during organ formation**
1222 **induced by addition of lanolin containing 1mM IAA on *pin1-613* apexes.** From left
1223 to right, pre-treatment, 24, 48, 72, and 96 hours after treatment. Four representative
1224 samples are shown top to bottom. Arrows indicate the lanolin paste at the 24-hour time-
1225 point. All samples were imaged with identical settings. Scale bars 25µm.

1226

1227

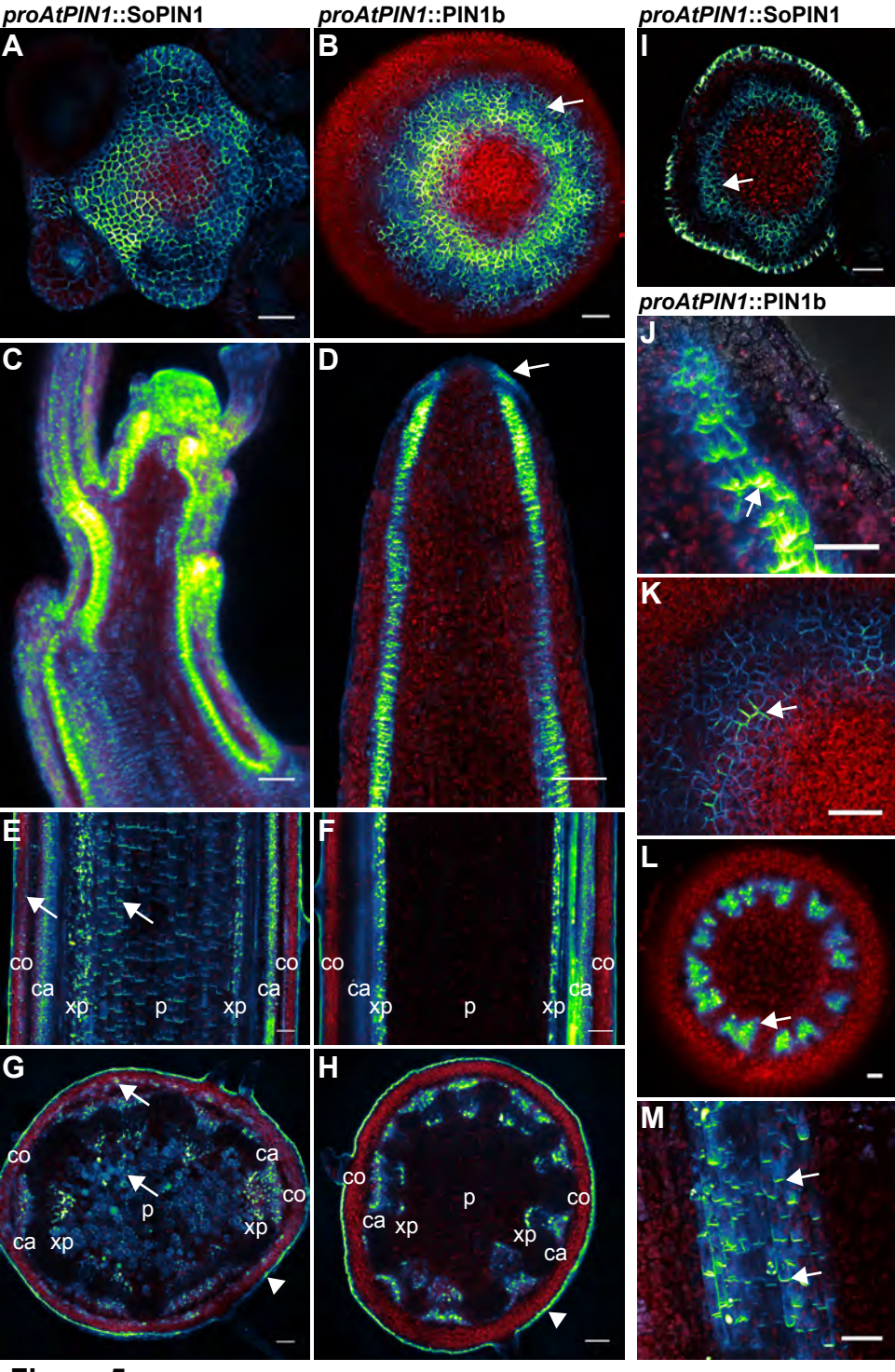
*proAtPIN1*::SoPIN1
*proAtPIN1*::PIN1b
*proAtPIN1*::SoPIN1
*proAtPIN1*::PIN1b
A
B
C
D
E
F
G
H
I
J
K
L
M
co
ca
xp
p

**Figure 5**

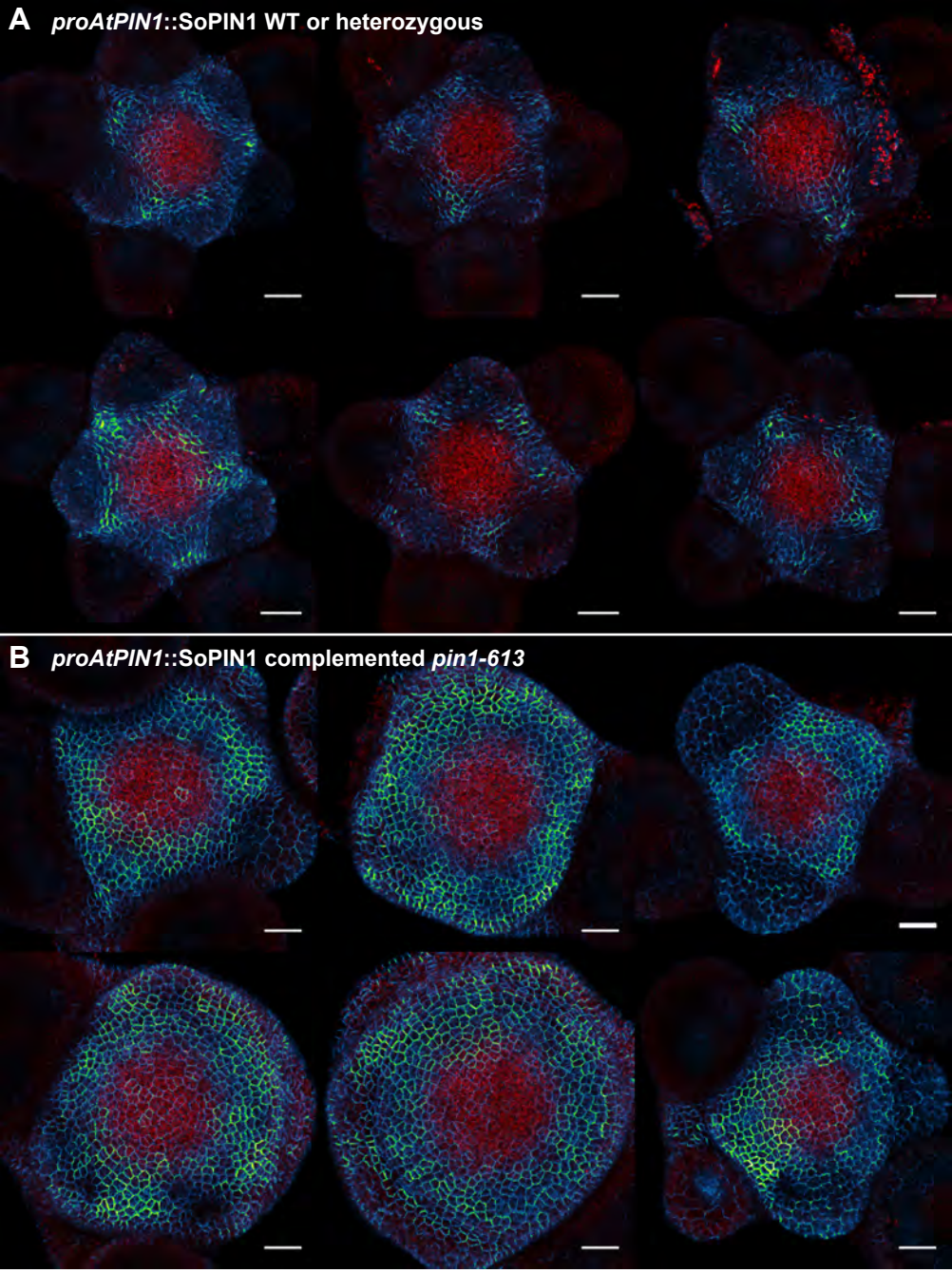


**Figure 5 - supplement 1**

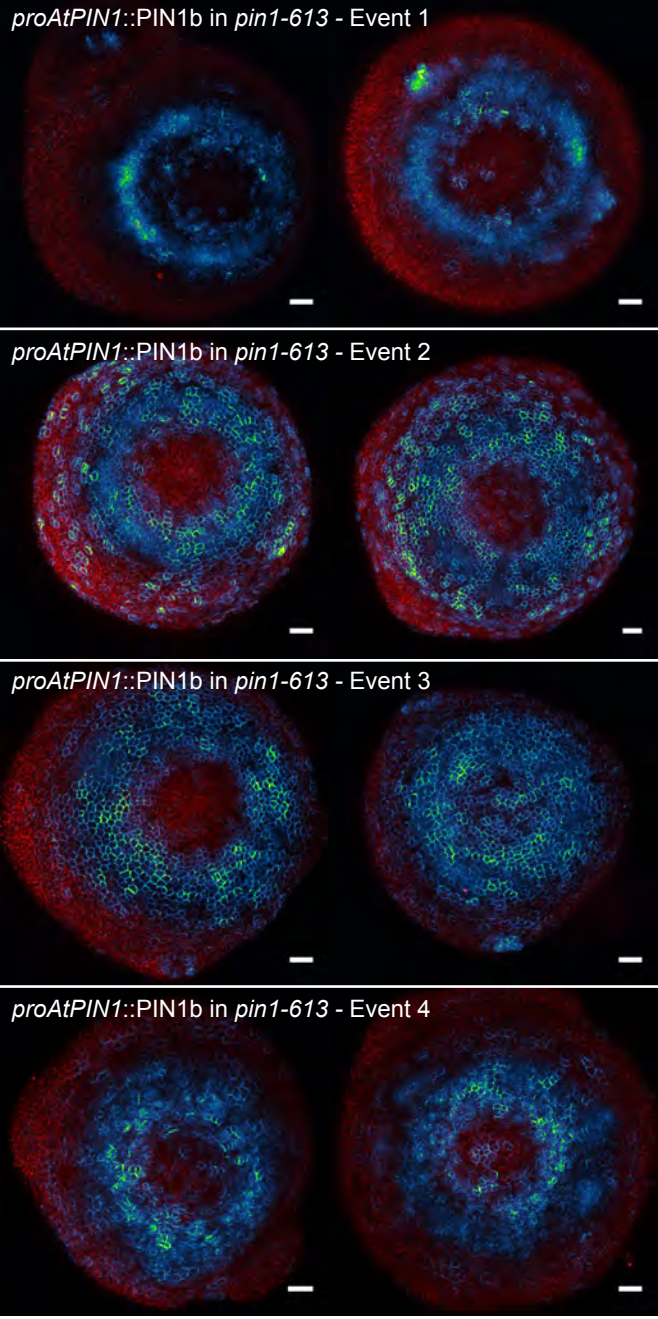


**Figure 5 - supplement 2**

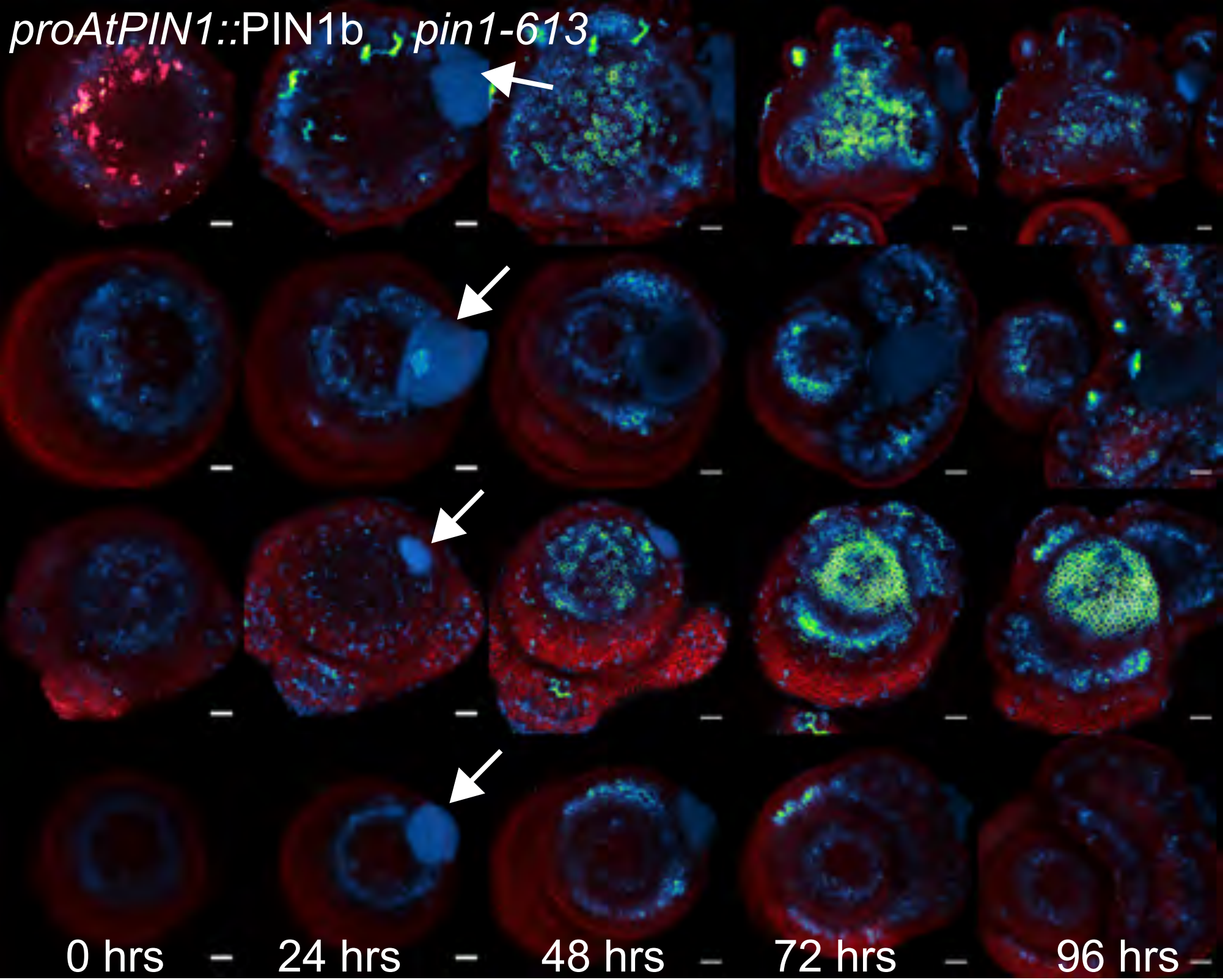


**Figure 5 - supplement 3**

1228 **Figure 6. SoPIN1 and PIN1b show different behaviors under *proAtML1*-driven**
1229 **expression.** Maximum projections of *proAtML1::*LhG4 driving pOP::SoPIN1 or
1230 pOP::PIN1b (*proAtML1*>>SoPIN1 and *proAtML1*>>PIN1b) in wild-type Landsberg
1231 *erecta* (L*er)* **(A-D),** and *pin1-4* **(E-L)** inflorescence meristems and basal internodes. **(A)**
1232 SoPIN1 and **(B)** PIN1b maximum projections of wild-type L*er* inflorescence meristems.
1233 I3, I2, I1, and P1 primordia are indicated. White boxes around each I2 primordium
1234 indicate the regions detailed in **(C-D).** Asterisk in **(C)** indicates convergence point. Arrow
1235 in **(D)** indicates punctate PIN1b. **(E)** SoPIN1 and **(F)** PIN1b maximum projections of
1236 complemented *pin1-4* meristems. I3, I2, I1, and P1 primordia are indicated. White boxes
1237 around each I2 primordia indicate the regions detailed in **(G-H)**. Asterisks mark
1238 convergence points in **(G)** and **(H)**. Red signal in **(C,D,G,H)** is cell wall propidium iodide
1239 staining. See Figure 6 – supplement 1 for additional samples of *proAtML1*>>SoPIN1
1240 and Figure 6 – supplement 2 for additional samples of *proAtML1*>>PIN1b in both WT
1241 and *pin1-4* meristems. See Figure 6 - supplement 3 for details of PIN1b epidermal
1242 intracellular localization in WT and *pin1-4* meristem apexes. **(I-J)** Tiled maximum
1243 projections of cross hand-sections of the basal internode of SoPIN1 **(I)** and PIN1b **(J)** -
1244 complemented *pin1-4* plants showing PIN signal in the outer cortex layers (arrows). Red
1245 signal in **(I-J)** is chlorophyll auto-florescence. **(K-L)** Epidermal maximum projections
1246 showing rootward polarized PIN localization (arrows) in the basal internode of SoPIN1
1247 **(K),** and PIN1b **(L)** -complemented *pin1-4* plants. Scale bars: 25μm in **(A-H)**. 100μm in
1248 **(I-L)**.
1249

1250 **Figure 6 – supplement 1. *proAtML1*>>SoPIN1 representative meristem maximum**
1251 **projections. (A)** *proAtML1*>>SoPIN1 expression in three different wild-type L*er*
1252 meristems. **(B)** *proAtML1*>>SoPIN1 expression in three different complemented *pin1-4*
1253 meristems. Capture settings are identical in all samples. Scale bars: 25µm.
1254
1255 **Figure 6 – supplement 2. *proAtML1*>>PIN1b representative meristem maximum**
1256 **projections. (A)** *proAtML1*>>PIN1b expression in three different wild-type L*er*
1257 meristems. **(B)** *proAtML1*>>PIN1b expression in three different complemented *pin1-4*
1258 meristems. Capture settings are identical in all samples. Scale bars: 25µm.
1259
1260 **Figure 6 – supplement 3. Subcellular localization of PIN1b in wild-type (L*er*) and**
1261 ***pin1-4* meristems. (A)** Wild-type (L*er*) meristem expressing *proAtML1*>>PIN1b. Boxes
1262 numbered 1-3 indicate the positions of detail images in **(B-D). (B)** Organ boundary. **(C)**
1263 Incipient organ. **(D)** Meristem apex. **(E)** *pin1-4* meristem complemented by
1264 *proAtML1*>>PIN1b. Boxes numbered 1-3 indicate the positions of detail images in (**F-H).**
1265 **(F)** Meristem apex. **(G)** Organ boundary. **(H)** Convergence point, indicated by asterisk.
1266 Red signal is FM4-64 vital stain. Scale bars: 5µm.
1267
1268

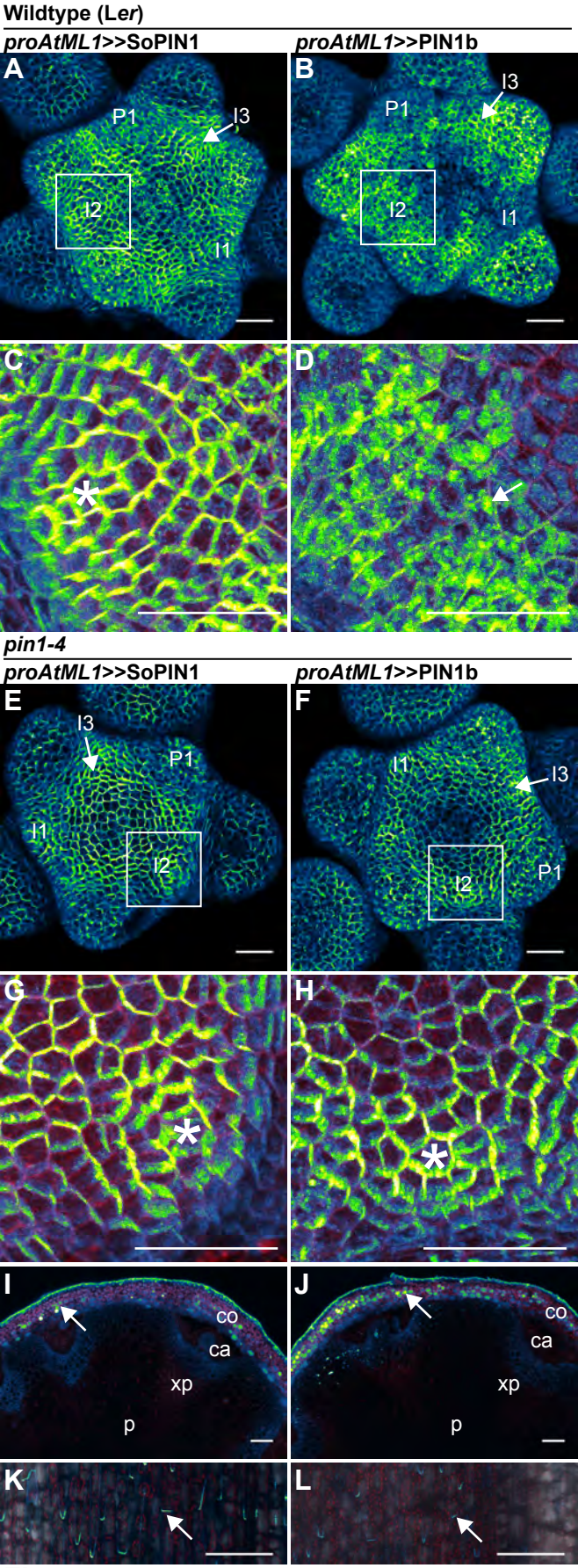
Wildtype (Ler)
proAtML1>>SoPIN1
proAtML1>>PIN1b
A
B
P1
I3
I2
I1
C
D
pin1-4
proAtML1>>SoPIN1
proAtML1>>PIN1b
E
F
G
H
I
J
co
ca
xp
p
K
L

Figure 6

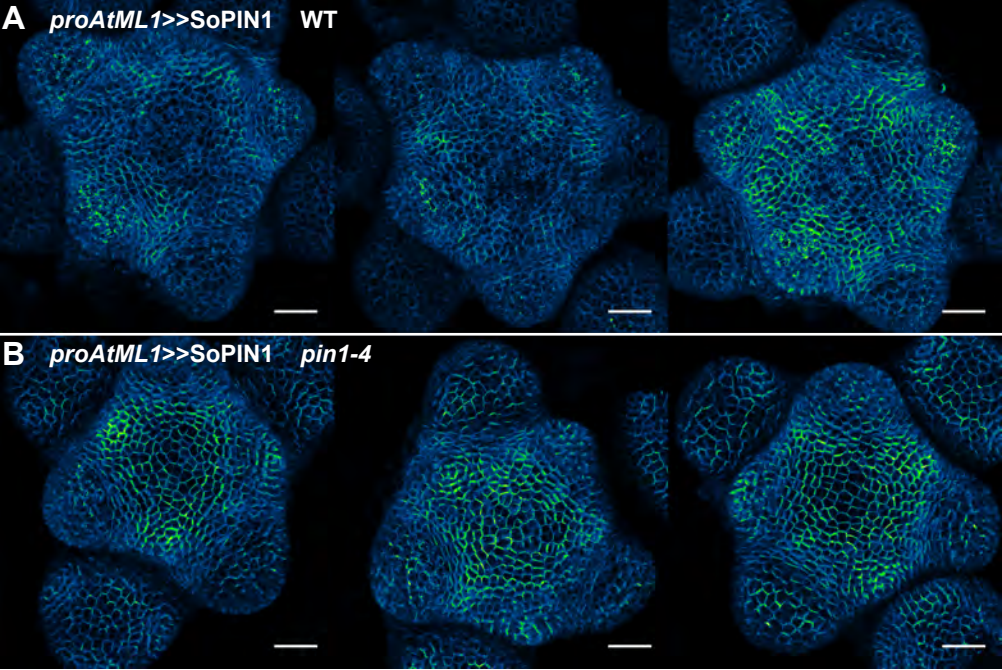


**Figure 6 - supplement 1 - *proAtML1*>>SoPIN1**

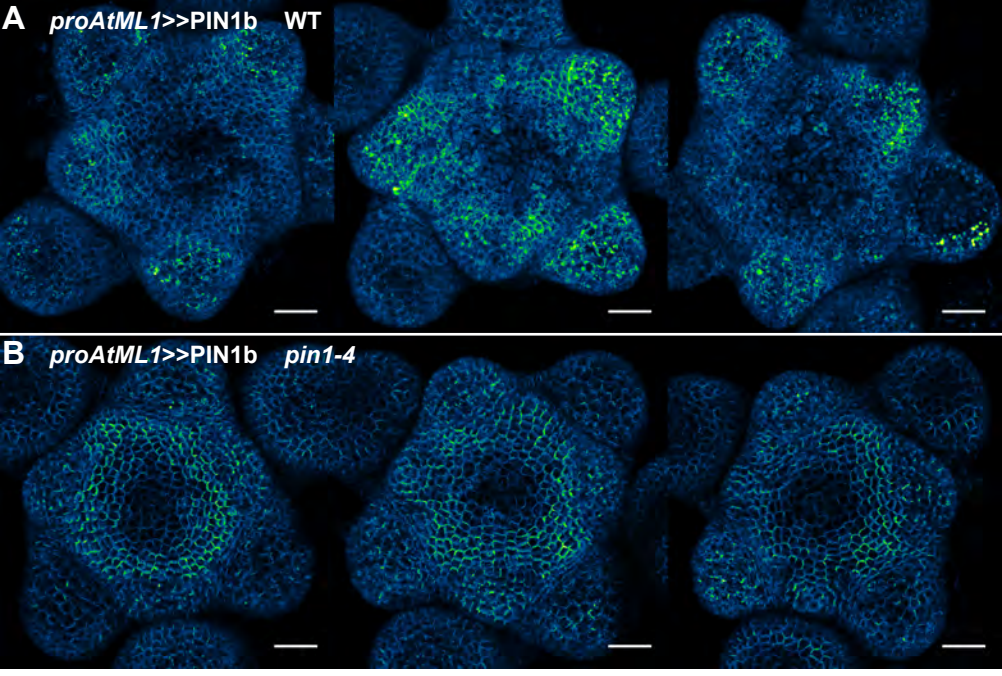


**Figure 6 - supplement 2 - *proAtML1*>>PIN1b**

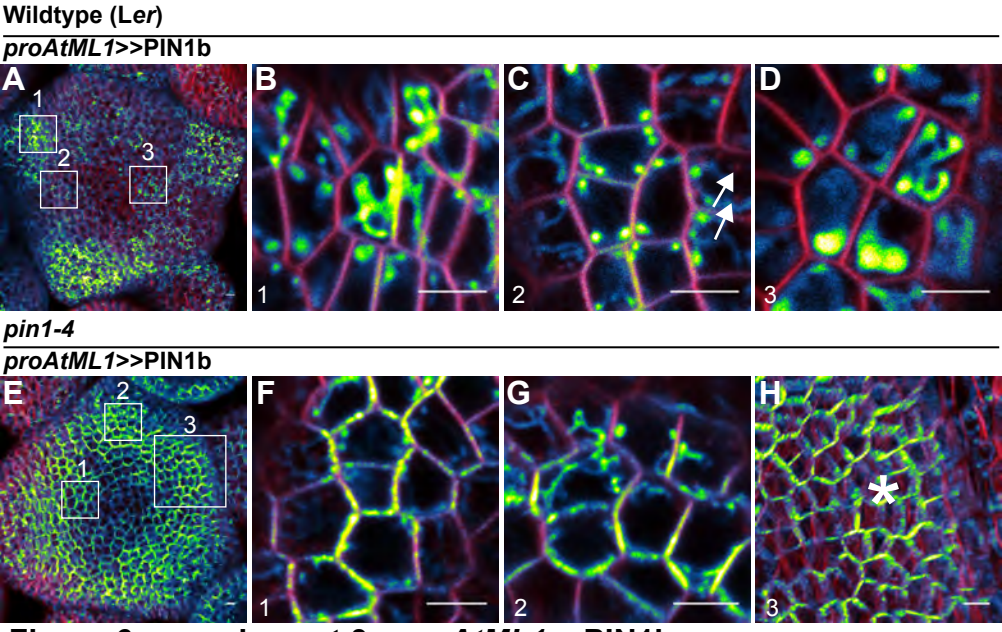


**Figure 6 - supplement 3 - *proAtML1*>>PIN1b**

1269 **Figure 7. AtPIN1 protein immuno-localization in wild-type, *pin1-613,* and *pin1-4***
1270 **meristems. (A)** AtPIN1 protein accumulation in wild-type L*er* inflorescence apex shows
1271 polar PIN protein at the sites of initiating organs (asterisk), and during vein patterning
1272 below the apex (arrow). **(B)** No AtPIN1 protein is detected in *pin1-613* null mutant pin-
1273 formed apexes. **(C)** Abundant AtPIN1 protein is detected in *pin1-4* pin-formed apexes,
1274 primarily in provascular tissues below the meristem apex (arrow). Box shows region of
1275 detail in **(D). (D)** Detail of boxed area shown in **(C)**. AtPIN1 protein in *pin1-4*
1276 accumulates in a perinuclear domain (arrow). All samples are 9μm longitudinal sections.
1277 Scale bars: 25μm in A-C, and 5μm in D.

1278

1279

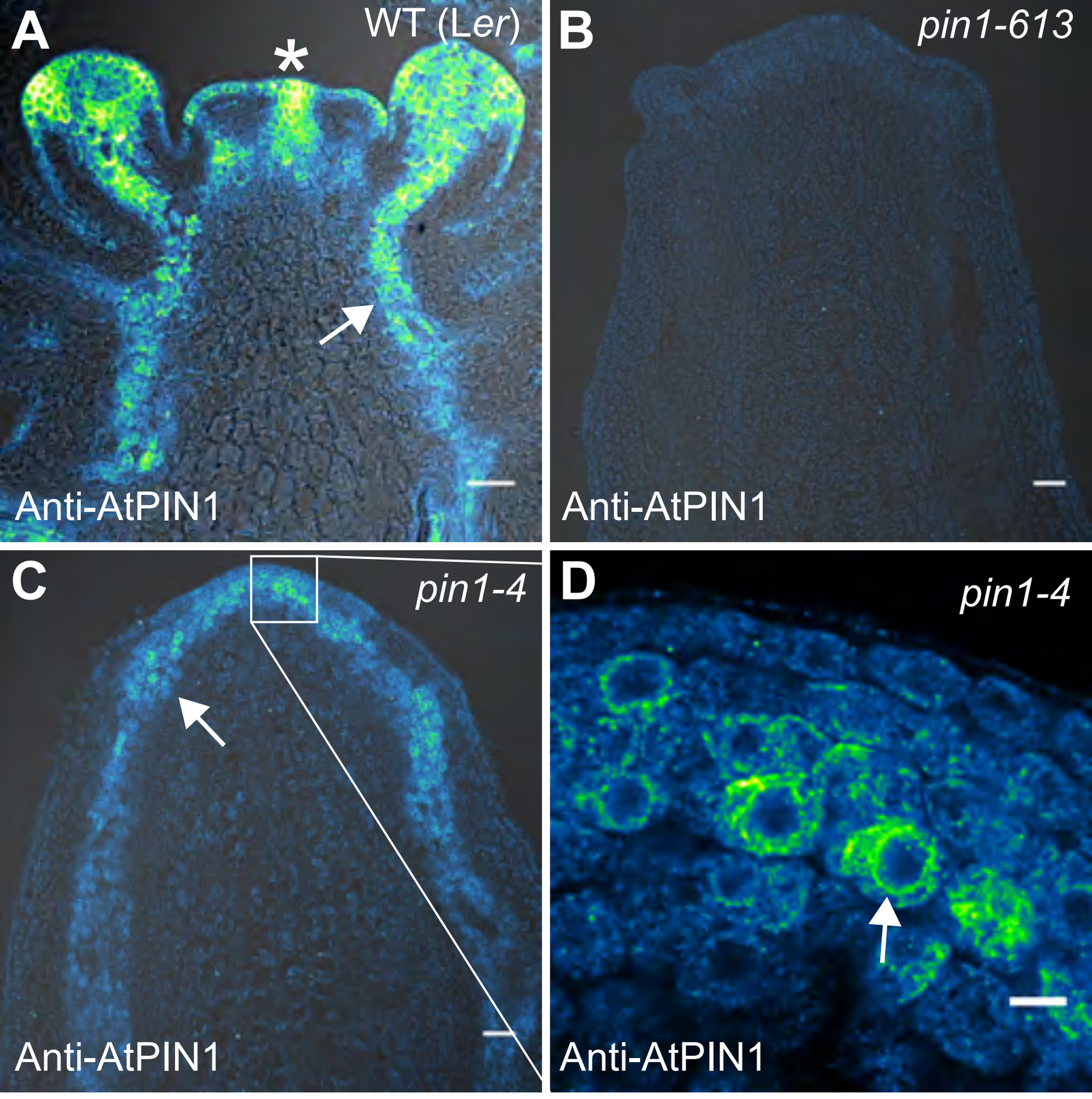
A
WT (Ler)
*
Anti-AtPIN1
B
pin1-613
Anti-AtPIN1
C
pin1-4
Anti-AtPIN1
D
pin1-4
Anti-AtPIN1

**Figure 7**

1280 **Figure 8. Both SoPIN1 and PIN1b can complement Arabidopsis *pin1-4* under**
1281 ***proAtML1*-driven expression. (A)** From left to right, wild-type L*er, proAtML1*>>PIN1b
1282 complemented *pin1-4, proAtML1*>>SoPIN1 complemented *pin1-4, and pin1-4 alone.*
1283 Arrow indicates barren pin inflorescence in *pin1-4*. See Figure 8 – supplement 1 for
1284 inflorescence phenotypes. **(B)** Box-plot of bulk auxin transport (counts per minute,
1285 CPM) through basal internodes 1cm above the rosette of 40-day-old Arabidopsis
1286 inflorescence stems (n=16 each genotype). Samples with different letters are
1287 significantly different from each other (ANOVA, Tukey HSD, $p < 0.05$). See Figure 8 -
1288 Source Data 1 for source data. **(C)** Box-plot of stem cross-sectional area (square mm)
1289 of the basal internode 1cm above the rosette (n=12 each genotype). Samples with
1290 different letters are significantly different from each other. (ANOVA, Tukey HSD, $p <$
1291 $0.05$). See Figure 8 - Source Data 2 for source data. Representative Toluidine Blue O
1292 stained hand cross-sections are shown above each box for each genotype. Scale bars:
1293 1cm in **(A)**. 500µm in **(C).**
1294
1295 **Figure 8 – supplement 1. *proAtML1*>>SoPIN1 and *proAtML1*>>PIN1b**
1296 **complemented *pin1-4* inflorescence phenotypes. (A)** Wild-type L*er*, **(B)**
1297 *proAtML1*>>SoPIN1 complemented *pin1-4,* and **(C)** *proAtML1*>>PIN1b complemented
1298 *pin1-4* inflorescence apexes. Scale bars: 1mm.
1299
1300 **Figure 8 - Source Data 1. Source data for Figure 8B auxin transport assays.**
1301

1302 **Figure 8 - Source Data 2. Source data for Figure 8C stem cross-sectional area**

1303 **measurements.**

1304

1305

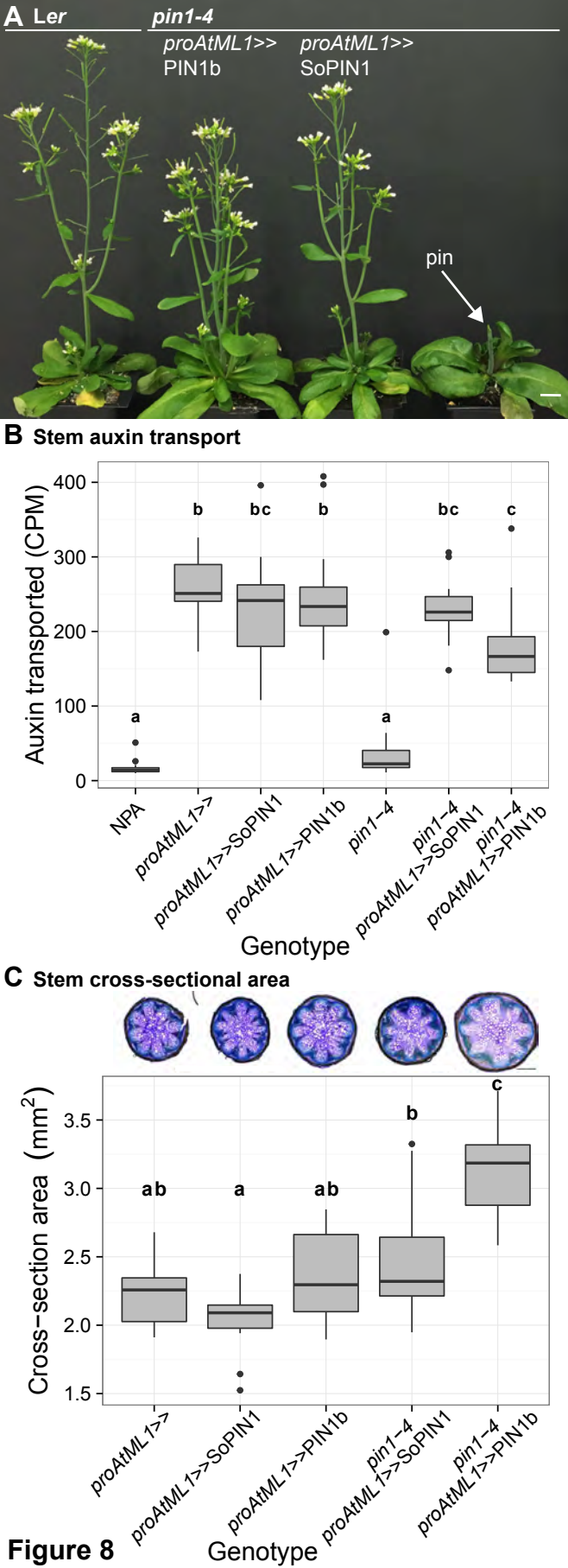
A
Ler
pin1-4
proAtML1>>
PIN1b
proAtML1>>
SoPIN1
pin
B
Stem auxin transport
Auxin transported (CPM)
400
300
200
100
0
a
b
bc
b
a
bc
c
NPA
proAtML1>>
proAtML1>>SoPIN1
proAtML1>>PIN1b
pin1−4
pin1−4
proAtML1>>SoPIN1
pin1−4
proAtML1>>PIN1b
Genotype
C
Stem cross-sectional area
Cross−section area (mm2)
3.5
3.0
2.5
2.0
1.5
ab
a
ab
b
c
proAtML1>>
proAtML1>>SoPIN1
proAtML1>>PIN1b
pin1−4
proAtML1>>SoPIN1
pin1−4
proAtML1>>PIN1b
Genotype

**Figure 8**

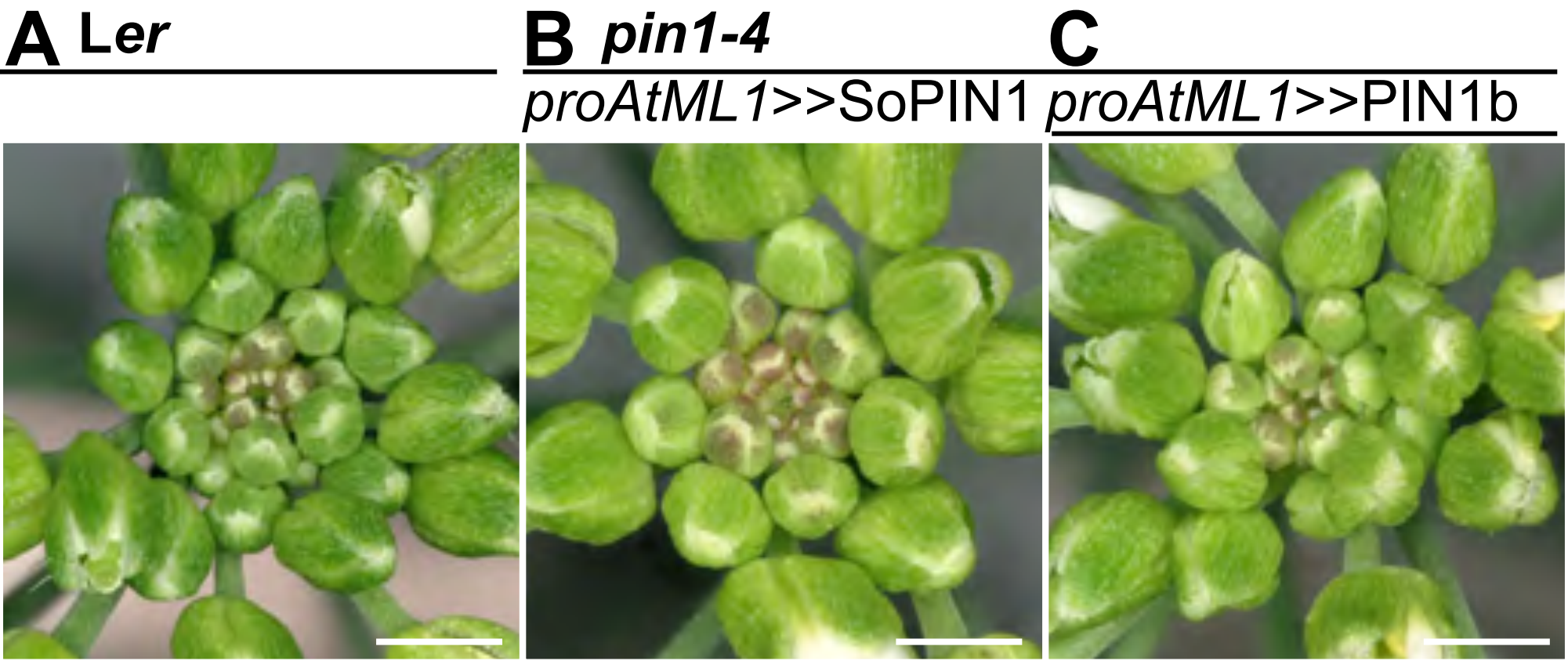


# Figure 8 - supplement 1

1306 **Figure 9. Heterologous expression visual summary: Functional distinction**
1307 **between PIN auxin efflux proteins during development.** Polarized SoPIN1 is
1308 represented by green lines, polarized PIN1b by blue lines, un-polarized PIN1b by blue
1309 circles, and the putative partially functional *pin1-4* protein is indicated by magenta
1310 circles. Red arrows indicate measured auxin transport in the basal internode, while red
1311 bar-headed lines indicated reduced transport. Black arrows represent polarized PIN
1312 patterns. Convergence points are marked with asterisks. **(A)** When expressed in both
1313 the epidermis and internal tissues with *proAtPIN1* in wild-type Col-0, SoPIN1 forms
1314 convergent polarization patterns in the epidermis and is partially able to rescue the
1315 organ initiation phenotypes and bulk transport in null *pin1-613* mutants. **(B)** When
1316 SoPIN1 is expressed only in the epidermis from the *proAtML1* promoter, it forms
1317 convergence points in the wild-type background and is able to rescue more fully the
1318 organ initiation phenotypes of the *pin1-4* single amino acid change mutation in L*er.* **(C)**
1319 In contrast, when PIN1b is expressed in both the epidermis and internal tissues from the
1320 *proAtPIN1* promoter in wild-type Col-0, it accumulates mostly in the internal tissues, and
1321 is unable to complement the *pin1-613* organ initiation phenotype. It is also unable to
1322 transport auxin through stem segments, despite apparently AtPIN1-like accumulation
1323 and polarization in the stem. **(D)** When PIN1b is expressed in the epidermis from the
1324 *proAtML1* promoter it does not form convergent polarization patterns and is often un-
1325 polarized in the wild-type *Ler* background (blue ovals), but it does in the *pin1-4*
1326 background, where it is able to rescue the defective organ initiation phenotype and
1327 mediate bulk transport. See Figure 9 - supplement 1 for a protein alignment comparing
1328 AtPIN1 to other PIN1-clade protein sequences from diverse angiosperms.

1329

1330 **Figure 9 - supplement 1. Brassicaceae-specific PIN1 domains. (A)** Wrapped protein
1331 alignment showing PIN1 clade members from across the angiosperms. Grass PIN1a
1332 proteins are indicated with grey rectangle, grass PIN1b proteins are indicated with black
1333 rectangle, and Brassicaceae PIN1 proteins are indicated with red rectangle. Domains
1334 that are unique to the Brassicaceae family proteins are indicated by transparent red
1335 boxes over the alignment. **(B)** Sequenced angiosperm species and version numbers,
1336 from https://phytozome.jgi.doe.gov. Species used in the alignment in **(A)** are indicated
1337 with green circles. See Figure 9 - Source Data 1 for source data.

1338

1339 **Figure 9 - Source Data 1. FASTA alignment source data for Figure 9 - supplement**
1340 **1.**

1341

1342 **Table 1. Primers.** See methods for usage.

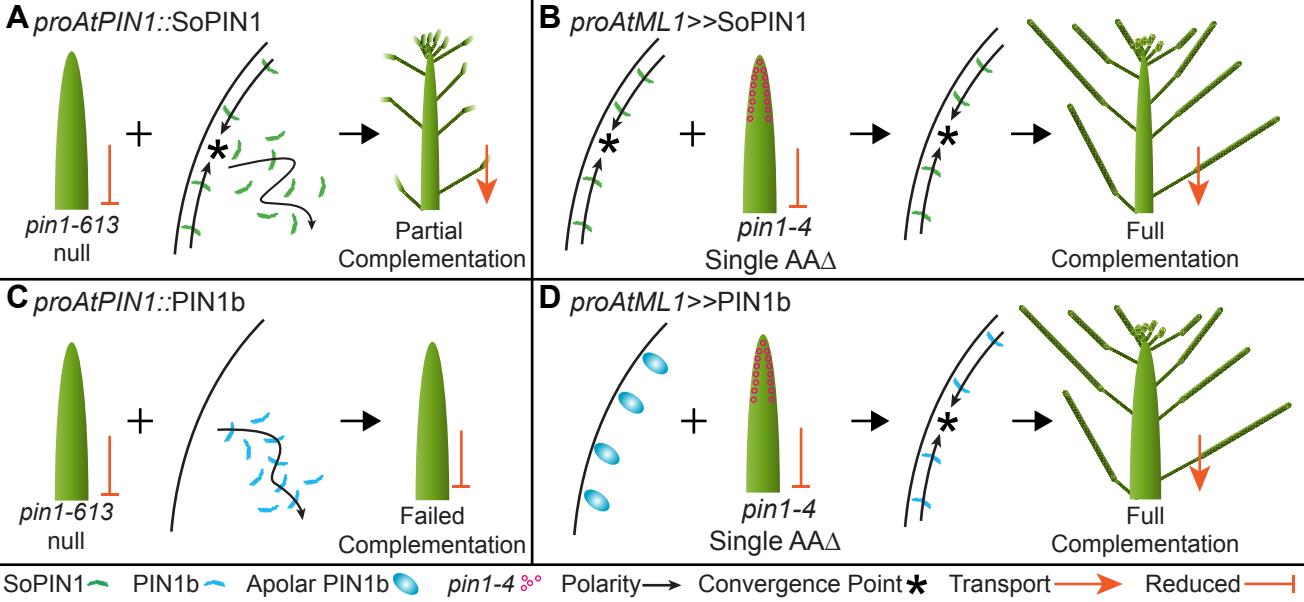
A proAtPIN1::SoPIN1
pin1-613
null
Partial
Complementation
B proAtML1>>SoPIN1
pin1-4
Single AAΔ
Full
Complementation
C proAtPIN1::PIN1b
pin1-613
null
Failed
Complementation
D proAtML1>>PIN1b
pin1-4
Single AAΔ
Full
Complementation
SoPIN1
PIN1b
Apolar PIN1b
pin1-4
Polarity
Convergence Point
Transport
Reduced

**Figure 9**

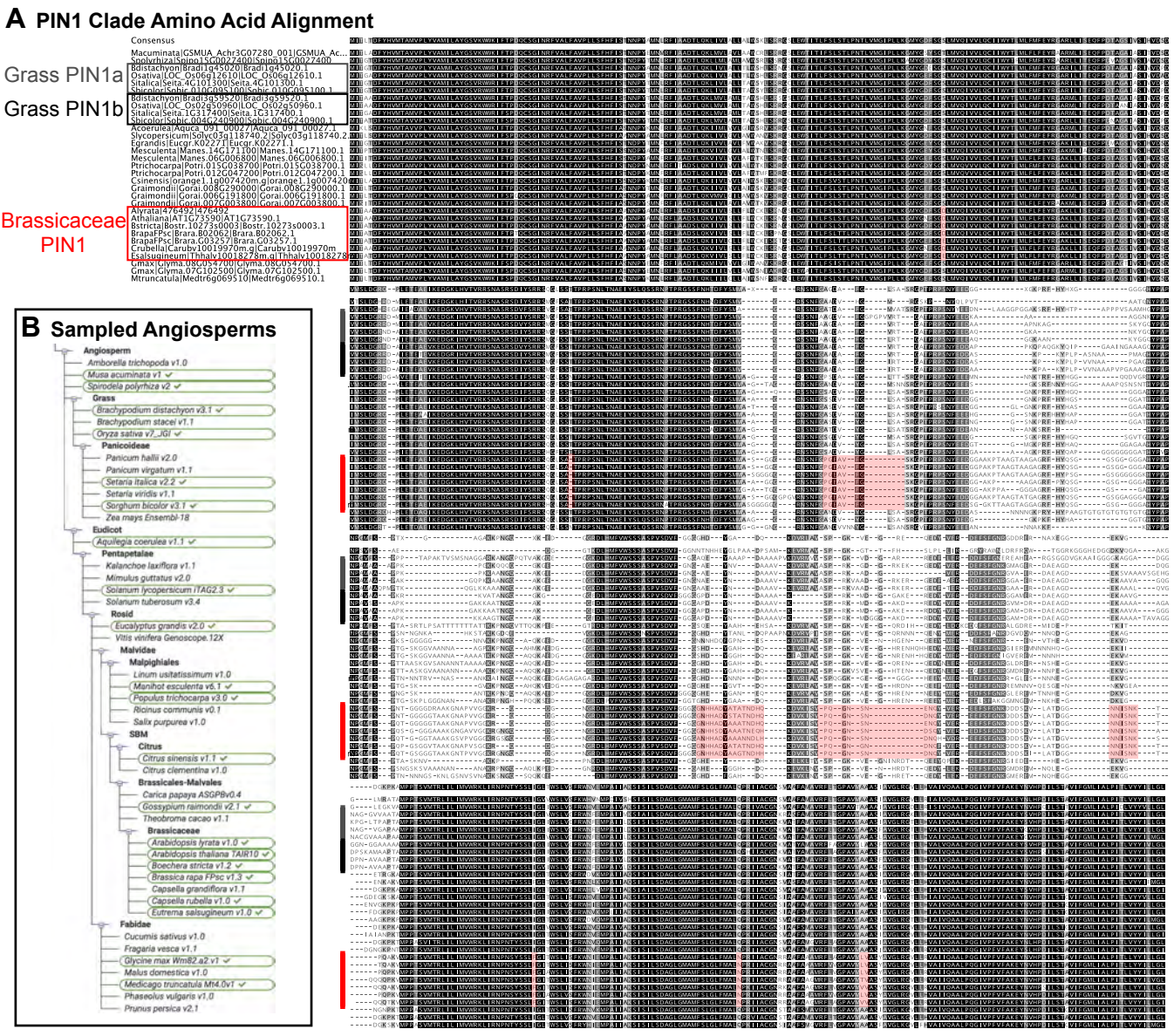


**Figure 9 - supplement 1**

**Table 1: Primers**

| ID# | Name | Sequence | Purpose |
|---|---|---|---|
| 1 | 524_Bradi4g26300_4230_F | CGTTCCGTGTTGATTCCGATG | *sopin1-1* genotyping with HgaI digestion |
| 2 | 525_Bradi4g26300_4923_R | CTGGAGTAGGTGTTGGGGTTC | *sopin1-1* genotyping with HgaI digestion |
| 3 | 526_Cas9_8622_F | TCCCAGAGAAGTACAAGGAGATCT | Cas9 Genotyping |
| 4 | 527_Cas9_9159_R | TTGTACACGGTGAAGTACTCGTAG | Cas9 Genotyping |
| 5 | 104_BdPIN_11_QPCR_F | ACAACCCTTACGCCATGAAC | *pin1a-1* genotyping with NcoI digestion |
| 6 | 473_PIN1a_dom1_shortR | CACACGAACATGTGCAGGTC | *pin1a-1* genotyping with NcoI digestion |
| 7 | 541_Bradi3g59520_PIN1b_5084_F | TGATGCTCTTCATGTTCGAGTACC | *pin1b-1* genotyping with mboI digestion |
| 8 | 542_Bradi3g59520_PIN1b_5838_R | GGAGTAAACTACGTTGTGACAAGG | *pin1b-1* genotyping with mboI digestion |
| 9 | 019 - Ubi-1 Prom attB4 F | GGGGACAACTTTGTATAGAAAAGTTGCTGCAGTGCAGCGTGACCCGG | pZmUbi amplification for cloning |
| 10 | 020 - Ubi-1 Prom attB1 R | GGGGACTGCTTTTTTGTACAAACTTGCTGCAGAAGTAACACCAAACA | pZmUbi amplification for cloning |
| 11 | PIN1pro-GW-F | GGGGACAACTTTGTATAGAAAAGTTGTTACCCTCATCCATCATTAACTT | *proAtPIN1* amplification |
| 12 | PIN1pro-GW-R | GGGGACTGCTTTTTTGTACAAACTTGTCTTTTGTTCGCCGGAGAAGAGA | *proAtPIN1* amplification |
| 13 | 455 BdSoPIN1 cacc mRNA | TCACATCTGCTGCCGCTGCC | SoPIN1-Citrine coding region amplification |
| 14 | 302 - PIN_7 qPCR UTR R2 | AATCCCAAAAGCCGACATTG | SoPIN1-Citrine coding region amplification |
| 15 | 466 BdPIN1b cacc mRNA-2 | CACCTGTACACACTGCGGCGCT | PIN1b-Citrine coding region amplification |
| 16 | 308 - PIN_5 qPCR UTR R1 | ACTCGCTAACCAACCCCTTAATT | PIN1b-Citrine coding region amplification |
| 17 | MVR087 - pin1-613 RP (SALK_047613) | AATCATCACAGCCACTGATCC | *pin1-613* genotyping |
| 18 | MVR086 - pin1-613 LP (SALK_047613) | CAAAAACACCCCCAAAATTTC | *pin1-613* genotyping |
| 19 | MVR036 - LBb1.3 | ATTTTGCCGATTTCGGAAC | *pin1-613* genotyping |
| 20 | 344 - Citrine Seq R | GAAGCACATCAGGCCGTAG | PIN1b-Citrine and SoPIN1-Citrine genotyping |
| 21 | 524_Bradi4g26300_4230_F | CGTTCCGTGTTGATTCCGATG | SoPIN1-Citrine genotyping |
| 22 | 541_Bradi3g59520_PIN1b_5084_F | TGATGCTCTTCATGTTCGAGTACC | PIN1b-Citrine genotyping |
| 23 | 543_pin1-4_Aci_F | GCTTTTGCGGCGGCTATGAGATTTGT | *pin1-4* genotyping with AciI digestion |
| 24 | 544_pin1-4_Aci_R | GCTTCTGATTTAATTTGTGGGTTTTCA | *pin1-4* genotyping with AciI digestion |
| 25 | 076 - BASTA_F2 | CTTCAGCAGGTGGGTGTAGAG | ML1::LhG4 genotyping |
| 26 | 077 - BASTA_R2 | GAGACAAGCACGGTCAACTTC | ML1::LhG4 genotyping |